

# Elastic and Proton-Dissociative $\rho^0$ Photoproduction at HERA

ZEUS Collaboration

## Abstract

Elastic and proton-dissociative  $\rho^0$  photoproduction ( $\gamma p \rightarrow \rho^0 p$ ,  $\gamma p \rightarrow \rho^0 N$ , respectively, with  $\rho^0 \rightarrow \pi^+\pi^-$ ) has been studied in  $ep$  interactions at HERA for photon-proton centre-of-mass energies in the range  $50 < W < 100$  GeV and for  $|t| < 0.5$  GeV<sup>2</sup>, where  $t$  is the square of the four-momentum transfer at the proton vertex; the results on the proton-dissociative reaction are presented for masses of the dissociated proton system in the range  $M_N^2 < 0.1W^2$ . For the elastic process, the  $\pi^+\pi^-$  invariant mass spectrum has been investigated as a function of  $t$ . As in fixed target experiments, the  $\rho^0$  resonance shape is asymmetric; this asymmetry decreases with increasing  $|t|$ , as expected in models in which the asymmetry is ascribed to the interference of resonant and non-resonant  $\pi^+\pi^-$  production. The cross section has been studied as a function of  $W$ ; a fit to the resonant part with the form  $W^a$  gives  $a = 0.16 \pm 0.06$  (stat.)  $^{+0.11}_{-0.15}$  (syst.). The resonant part of the  $\gamma p \rightarrow \pi^+\pi^-p$  cross section is  $11.2 \pm 0.1$  (stat.)  $^{+1.1}_{-1.2}$  (syst.)  $\mu\text{b}$  at  $\langle W \rangle = 71.7$  GeV. The  $t$  dependence of the cross section can be described by a function of the type  $A_\rho \exp(-b_\rho|t| + c_\rho t^2)$  with  $b_\rho = 10.9 \pm 0.3$  (stat.)  $^{+1.0}_{-0.5}$  (syst.) GeV<sup>-2</sup> and  $c_\rho = 2.7 \pm 0.9$  (stat.)  $^{+1.9}_{-1.7}$  (syst.) GeV<sup>-4</sup>. The  $t$  dependence has also been studied as a function of  $W$  and a value of the slope of the pomeron trajectory  $\alpha_{\mathbb{P}}' = 0.23 \pm 0.15$  (stat.)  $^{+0.10}_{-0.07}$  (syst.) GeV<sup>-2</sup> has been deduced. The  $\rho^0$  spin density matrix elements  $r_{00}^{04}$ ,  $r_{1-1}^{04}$  and  $\Re[r_{10}^{04}]$  have been measured and found to be consistent with expectations based on  $s$ -channel helicity conservation. For proton-dissociative  $\pi^+\pi^-$  photoproduction in the  $\rho^0$  mass range, the distributions of the two-pion invariant mass,  $W$  and the polar and azimuthal angles of the pions in the helicity frame are the same within errors as those for the elastic process. The  $t$  distribution has been fitted to an exponential function with a slope parameter  $5.8 \pm 0.3$  (stat.)  $\pm 0.5$  (syst.) GeV<sup>-2</sup>. The ratio of the elastic to proton-dissociative  $\rho^0$  photoproduction cross section is  $2.0 \pm 0.2$  (stat.)  $\pm 0.7$  (syst.).

# The ZEUS Collaboration

J. Breitweg, M. Derrick, D. Krakauer, S. Magill, D. Mikunas, B. Musgrave, J. Repond, R. Stanek, R.L. Talaga, R. Yoshida, H. Zhang

*Argonne National Laboratory, Argonne, IL, USA <sup>p</sup>*

M.C.K. Mattingly

*Andrews University, Berrien Springs, MI, USA*

F. Anselmo, P. Antonioli, G. Bari, M. Basile, L. Bellagamba, D. Boscherini, A. Bruni, G. Bruni, G. Cara Romeo, G. Castellini<sup>1</sup>, M. Chiarini, L. Cifarelli<sup>2</sup>, F. Cindolo, A. Contin, M. Corradi, S. De Pasquale, I. Gialas<sup>3</sup>, P. Giusti, G. Iacobucci, G. Laurenti, G. Levi, A. Margotti, T. Massam, R. Nania, C. Nemoz<sup>4</sup>, F. Palmonari, A. Pesci, A. Polini, F. Ricci, G. Sartorelli, Y. Zamora Garcia<sup>5</sup>, A. Zichichi

*University and INFN Bologna, Bologna, Italy <sup>f</sup>*

C. Amelung, A. Bornheim, I. Brock, K. Coböken, J. Crittenden, R. Deffner, M. Eckert, M. Grothe, H. Hartmann, K. Heinloth, L. Heinz, E. Hilger, H.-P. Jakob, U.F. Katz, R. Kerger, E. Paul, M. Pfeiffer, Ch. Rembser<sup>6</sup>, J. Stamm, R. Wedemeyer<sup>7</sup>, H. Wieber

*Physikalisches Institut der Universität Bonn, Bonn, Germany <sup>c</sup>*

D.S. Bailey, S. Campbell-Robson, W.N. Cottingham, B. Foster, R. Hall-Wilton, M.E. Hayes, G.P. Heath, H.F. Heath, J.D. McFall, D. Piccioni, D.G. Roff, R.J. Tapper

*H.H. Wills Physics Laboratory, University of Bristol, Bristol, U.K. <sup>o</sup>*

M. Arneodo<sup>8</sup>, R. Ayad, M. Capua, A. Garfagnini, L. Iannotti, M. Schioppa, G. Susinno

*Calabria University, Physics Dept.and INFN, Cosenza, Italy <sup>f</sup>*

J.Y. Kim, J.H. Lee, I.T. Lim, M.Y. Pac<sup>9</sup>

*Chonnam National University, Kwangju, Korea <sup>h</sup>*

A. Caldwell<sup>10</sup>, N. Cartiglia, Z. Jing, W. Liu, B. Mellado, J.A. Parsons, S. Ritz<sup>11</sup>, S. Sampson, F. Sciulli, P.B. Straub, Q. Zhu

*Columbia University, Nevis Labs., Irvington on Hudson, N.Y., USA <sup>q</sup>*

P. Borzemski, J. Chwastowski, A. Eskreys, J. Figiel, K. Klimek, M.B. Przybycień, L. Zawiejski

*Inst. of Nuclear Physics, Cracow, Poland <sup>j</sup>*

L. Adamczyk<sup>12</sup>, B. Bednarek, M. Bukowy, A. Czermak, K. Jeleń, D. Kisielewska, T. Kowalski, M. Przybycień, E. Rulikowska-Zarebska, L. Suszycki, J. Zając

*Faculty of Physics and Nuclear Techniques, Academy of Mining and Metallurgy, Cracow, Poland <sup>j</sup>*

Z. Duliński, A. Kotański

*Jagellonian Univ., Dept. of Physics, Cracow, Poland <sup>k</sup>*

G. Abbiendi<sup>13</sup>, L.A.T. Bauerdick, U. Behrens, H. Beier, J.K. Bienlein, G. Cases<sup>14</sup>, O. Deppe, K. Desler, G. Drews, U. Fricke, D.J. Wilkinson, C. Glasman, P. Göttlicher, T. Haas, W. Hain, D. Hasell, K.F. Johnson<sup>15</sup>, M. Kasemann, W. Koch, U. Kötz, H. Kowalski, J. Labs, L. Lindemann, B. Löhr, M. Löwe<sup>16</sup>, O. Mańczak, J. Milewski, T. Monteiro<sup>17</sup>, J.S.T. Ng<sup>18</sup>, D. Notz, K. Ohrenberg<sup>19</sup>, I.H. Park<sup>20</sup>, A. Pellegrino, F. Pelucchi, K. Piotrkowski, M. Roco<sup>21</sup>, M. Rohde, J. Roldán, J.J. Ryan, A.A. Savin, U. Schneekloth, O. Schwarzer, F. Selonke, B. Surrow, E. Tassi, T. Voß<sup>22</sup>, D. Westphal, G. Wolf, U. Wollmer<sup>23</sup>, C. Youngman, A.F. Żarnecki, W. Zeuner  
*Deutsches Elektronen-Synchrotron DESY, Hamburg, Germany*

B.D. Burow, H.J. Grabosch, A. Meyer, S. Schlenstedt  
*DESY-IfH Zeuthen, Zeuthen, Germany*

G. Barbagli, E. Gallo, P. Pelfer  
*University and INFN, Florence, Italy <sup>f</sup>*

G. Anzivino<sup>24</sup>, G. Maccarrone, L. Votano  
*INFN, Laboratori Nazionali di Frascati, Frascati, Italy <sup>f</sup>*

A. Bamberger, S. Eisenhardt, P. Markun, T. Trefzger<sup>25</sup>, S. Wölffe  
*Fakultät für Physik der Universität Freiburg i.Br., Freiburg i.Br., Germany <sup>c</sup>*

J.T. Bromley, N.H. Brook, P.J. Bussey, A.T. Doyle, N. Macdonald, D.H. Saxon, L.E. Sinclair, E. Strickland, R. Waugh  
*Dept. of Physics and Astronomy, University of Glasgow, Glasgow, U.K. <sup>o</sup>*

I. Bohnet, N. Gendner, U. Holm, A. Meyer-Larsen, H. Salehi, K. Wick  
*Hamburg University, I. Institute of Exp. Physics, Hamburg, Germany <sup>c</sup>*

L.K. Gladilin<sup>26</sup>, D. Horstmann, D. Kçira<sup>27</sup>, R. Klanner, E. Lohrmann, G. Poelz, W. Schott<sup>28</sup>, F. Zetsche  
*Hamburg University, II. Institute of Exp. Physics, Hamburg, Germany <sup>c</sup>*

T.C. Bacon, I. Butterworth, J.E. Cole, G. Howell, B.H.Y. Hung, L. Lamberti<sup>29</sup>, K.R. Long, D.B. Miller, N. Pavel, A. Prinias<sup>30</sup>, J.K. Sedgbeer, D. Sideris, R. Walker  
*Imperial College London, High Energy Nuclear Physics Group, London, U.K. <sup>o</sup>*

U. Mallik, S.M. Wang, J.T. Wu  
*University of Iowa, Physics and Astronomy Dept., Iowa City, USA <sup>p</sup>*

P. Cloth, D. Filges  
*Forschungszentrum Jülich, Institut für Kernphysik, Jülich, Germany*

J.I. Fleck<sup>6</sup>, T. Ishii, M. Kuze, I. Suzuki<sup>31</sup>, K. Tokushuku, S. Yamada, K. Yamauchi, Y. Yamazaki<sup>32</sup>  
*Institute of Particle and Nuclear Studies, KEK, Tsukuba, Japan <sup>g</sup>*

S.J. Hong, S.B. Lee, S.W. Nam<sup>33</sup>, S.K. Park  
*Korea University, Seoul, Korea <sup>h</sup>*

F. Barreiro, J.P. Fernández, G. García, R. Graciani, J.M. Hernández, L. Hervás<sup>6</sup>, L. Labarga, M. Martínez, J. del Peso, J. Puga, J. Terrón, J.F. de Trocóniz  
*Univer. Autónoma Madrid, Depto de Física Teórica, Madrid, Spain <sup>n</sup>*

F. Corriveau, D.S. Hanna, J. Hartmann, L.W. Hung, W.N. Murray, A. Ochs, M. Riveline,  
D.G. Stairs, M. St-Laurent, R. Ullmann

*McGill University, Dept. of Physics, Montréal, Québec, Canada <sup>a, b</sup>*

T. Tsurugai

*Meiji Gakuin University, Faculty of General Education, Yokohama, Japan*

V. Bashkirov, B.A. Dolgoshein, A. Stifutkin

*Moscow Engineering Physics Institute, Moscow, Russia <sup>l</sup>*

G.L. Bashindzhagyan, P.F. Ermolov, Yu.A. Golubkov, L.A. Khein, N.A. Korotkova, I.A. Korzhavina, V.A. Kuzmin, O.Yu. Lukina, A.S. Proskuryakov, L.M. Shcheglova<sup>34</sup>, A.N. Solomin<sup>34</sup>, S.A. Zotkin

*Moscow State University, Institute of Nuclear Physics, Moscow, Russia <sup>m</sup>*

C. Bokel, M. Botje, N. Brümmer, F. Chlebana<sup>21</sup>, J. Engelen, E. Koffeman, P. Kooijman, A. van Sighem, H. Tiecke, N. Tuning, W. Verkerke, J. Vosseveld, M. Vreeswijk<sup>6</sup>, L. Wiggers, E. de Wolf

*NIKHEF and University of Amsterdam, Amsterdam, Netherlands <sup>i</sup>*

D. Acosta, B. Bylsma, L.S. Durkin, J. Gilmore, C.M. Ginsburg, C.L. Kim, T.Y. Ling, P. Nylander, T.A. Romanowski<sup>35</sup>

*Ohio State University, Physics Department, Columbus, Ohio, USA <sup>p</sup>*

H.E. Blaikley, R.J. Cashmore, A.M. Cooper-Sarkar, R.C.E. Devenish, J.K. Edmonds, J. Große-Knetter<sup>36</sup>, N. Harnew, C. Nath, V.A. Noyes<sup>37</sup>, A. Quadt, O. Ruske, J.R. Tickner<sup>30</sup>, H. Uijterwaal, R. Walczak, D.S. Waters

*Department of Physics, University of Oxford, Oxford, U.K. <sup>o</sup>*

A. Bertolin, R. Brugnera, R. Carlin, F. Dal Corso, U. Dosselli, S. Limentani, M. Morandin, M. Posocco, L. Stanco, R. Stroili, C. Voci

*Dipartimento di Fisica dell' Università and INFN, Padova, Italy <sup>f</sup>*

J. Bulmahn, B.Y. Oh, J.R. Okrasinski, W.S. Toothacker, J.J. Whitmore

*Pennsylvania State University, Dept. of Physics, University Park, PA, USA <sup>q</sup>*

Y. Iga

*Polytechnic University, Sagamihara, Japan <sup>g</sup>*

G. D'Agostini, G. Marini, A. Nigro, M. Raso

*Dipartimento di Fisica, Univ. 'La Sapienza' and INFN, Rome, Italy <sup>f</sup>*

J.C. Hart, N.A. McCubbin, T.P. Shah

*Rutherford Appleton Laboratory, Chilton, Didcot, Oxon, U.K. <sup>o</sup>*

D. Epperson, C. Heusch, J.T. Rahn, H.F.-W. Sadrozinski, A. Seiden, R. Wichmann, D.C. Williams  
*University of California, Santa Cruz, CA, USA <sup>p</sup>*

H. Abramowicz<sup>38</sup>, G. Briskin, S. Dagan<sup>38</sup>, S. Kananov<sup>38</sup>, A. Levy<sup>38</sup>

*Raymond and Beverly Sackler Faculty of Exact Sciences, School of Physics, Tel-Aviv University, Tel-Aviv, Israel <sup>e</sup>*

T. Abe, T. Fusayasu, M. Inuzuka, K. Nagano, K. Umemori, T. Yamashita  
*Department of Physics, University of Tokyo, Tokyo, Japan*<sup>g</sup>

R. Hamatsu, T. Hirose, K. Homma<sup>39</sup>, S. Kitamura<sup>40</sup>, T. Matsushita  
*Tokyo Metropolitan University, Dept. of Physics, Tokyo, Japan*<sup>g</sup>

R. Cirio, M. Costa, M.I. Ferrero, S. Maselli, V. Monaco, C. Peroni, M.C. Petrucci, M. Ruspa,  
R. Sacchi, A. Solano, A. Staiano  
*Università di Torino, Dipartimento di Fisica Sperimentale and INFN, Torino, Italy*<sup>f</sup>

M. Dardo  
*II Faculty of Sciences, Torino University and INFN - Alessandria, Italy*<sup>f</sup>

D.C. Bailey, C.-P. Fagerstroem, R. Galea, G.F. Hartner, K.K. Joo, G.M. Levman, J.F. Martin,  
R.S. Orr, S. Polenz, A. Sabetfakhri, D. Simmons, R.J. Teuscher<sup>6</sup>  
*University of Toronto, Dept. of Physics, Toronto, Ont., Canada*<sup>a</sup>

J.M. Butterworth, C.D. Catterall, T.W. Jones, J.B. Lane, R.L. Saunders, M.R. Sutton, M. Wing  
*University College London, Physics and Astronomy Dept., London, U.K.*<sup>o</sup>

J. Ciborowski, G. Grzelak<sup>41</sup>, M. Kasprzak, K. Muchorowski<sup>42</sup>, R.J. Nowak, J.M. Pawlak,  
R. Pawlak, T. Tymieniecka, A.K. Wróblewski, J.A. Zakrzewski  
*Warsaw University, Institute of Experimental Physics, Warsaw, Poland*<sup>j</sup>

M. Adamus  
*Institute for Nuclear Studies, Warsaw, Poland*<sup>j</sup>

C. Coldewey, Y. Eisenberg<sup>38</sup>, D. Hochman, U. Karshon<sup>38</sup>  
*Weizmann Institute, Department of Particle Physics, Rehovot, Israel*<sup>d</sup>

W.F. Badgett, D. Chapin, R. Cross, S. Dasu, C. Foudas, R.J. Loveless, S. Mattingly, D.D. Reeder,  
W.H. Smith, A. Vaiciulis, M. Wodarczyk  
*University of Wisconsin, Dept. of Physics, Madison, WI, USA*<sup>p</sup>

A. Deshpande, S. Dhawan, V.W. Hughes  
*Yale University, Department of Physics, New Haven, CT, USA*<sup>p</sup>

S. Bhadra, W.R. Frisken, M. Khakzad, W.B. Schmidke  
*York University, Dept. of Physics, North York, Ont., Canada*<sup>a</sup>

<sup>1</sup> also at IROE Florence, Italy  
<sup>2</sup> now at Univ. of Salerno and INFN Napoli, Italy  
<sup>3</sup> now at Univ. of Crete, Greece  
<sup>4</sup> now at E.S.R.F., BP220, F-38043 Grenoble, France  
<sup>5</sup> supported by Worldlab, Lausanne, Switzerland  
<sup>6</sup> now at CERN  
<sup>7</sup> retired  
<sup>8</sup> also at University of Torino and Alexander von Humboldt Fellow at DESY  
<sup>9</sup> now at Dongshin University, Naju, Korea  
<sup>10</sup> also at DESY  
<sup>11</sup> Alfred P. Sloan Foundation Fellow  
<sup>12</sup> supported by the Polish State Committee for Scientific Research, grant No. 2P03B14912  
<sup>13</sup> supported by an EC fellowship number ERBFMBICT 950172  
<sup>14</sup> now at SAP A.G., Walldorf  
<sup>15</sup> visitor from Florida State University  
<sup>16</sup> now at ALCATEL Mobile Communication GmbH, Stuttgart  
<sup>17</sup> supported by European Community Program PRAXIS XXI  
<sup>18</sup> now at DESY-Group FDET  
<sup>19</sup> now at DESY Computer Center  
<sup>20</sup> visitor from Kyungpook National University, Taegu, Korea, partially supported by DESY  
<sup>21</sup> now at Fermi National Accelerator Laboratory (FNAL), Batavia, IL, USA  
<sup>22</sup> now at NORCOM Infosystems, Hamburg  
<sup>23</sup> now at Oxford University, supported by DAAD fellowship HSP II-AUFE III  
<sup>24</sup> now at University of Perugia, I-06100 Perugia, Italy  
<sup>25</sup> now at ATLAS Collaboration, Univ. of Munich  
<sup>26</sup> on leave from MSU, supported by the GIF, contract I-0444-176.07/95  
<sup>27</sup> supported by DAAD, Bonn  
<sup>28</sup> now a self-employed consultant  
<sup>29</sup> supported by an EC fellowship  
<sup>30</sup> PPARC Post-doctoral Fellow  
<sup>31</sup> now at Osaka Univ., Osaka, Japan  
<sup>32</sup> supported by JSPS Postdoctoral Fellowships for Research Abroad  
<sup>33</sup> now at Wayne State University, Detroit  
<sup>34</sup> partially supported by the Foundation for German-Russian Collaboration DFG-RFBR  
 (grant no. 436 RUS 113/248/3 and no. 436 RUS 113/248/2)  
<sup>35</sup> now at Department of Energy, Washington  
<sup>36</sup> supported by the Feodor Lynen Program of the Alexander von Humboldt foundation  
<sup>37</sup> Glasstone Fellow  
<sup>38</sup> supported by a MINERVA Fellowship  
<sup>39</sup> now at ICEPP, Univ. of Tokyo, Tokyo, Japan  
<sup>40</sup> present address: Tokyo Metropolitan College of Allied Medical Sciences, Tokyo 116, Japan  
<sup>41</sup> supported by the Polish State Committee for Scientific Research, grant No. 2P03B09308  
<sup>42</sup> supported by the Polish State Committee for Scientific Research, grant No. 2P03B09208

- <sup>a</sup> supported by the Natural Sciences and Engineering Research Council of Canada (NSERC)
- <sup>b</sup> supported by the FCAR of Québec, Canada
- <sup>c</sup> supported by the German Federal Ministry for Education and Science, Research and Technology (BMBF), under contract numbers 057BN19P, 057FR19P, 057HH19P, 057HH29P, 057SI75I
- <sup>d</sup> supported by the MINERVA Gesellschaft für Forschung GmbH, the German Israeli Foundation, and the U.S.-Israel Binational Science Foundation
- <sup>e</sup> supported by the German Israeli Foundation, and by the Israel Science Foundation
- <sup>f</sup> supported by the Italian National Institute for Nuclear Physics (INFN)
- <sup>g</sup> supported by the Japanese Ministry of Education, Science and Culture (the Monbusho) and its grants for Scientific Research
- <sup>h</sup> supported by the Korean Ministry of Education and Korea Science and Engineering Foundation
- <sup>i</sup> supported by the Netherlands Foundation for Research on Matter (FOM)
- <sup>j</sup> supported by the Polish State Committee for Scientific Research, grant No. 115/E-343/SPUB/P03/002/97, 2P03B10512, 2P03B10612, 2P03B14212, 2P03B10412
- <sup>k</sup> supported by the Polish State Committee for Scientific Research (grant No. 2P03B08308) and Foundation for Polish-German Collaboration
- <sup>l</sup> partially supported by the German Federal Ministry for Education and Science, Research and Technology (BMBF)
- <sup>m</sup> supported by the Fund for Fundamental Research of Russian Ministry for Science and Education and by the German Federal Ministry for Education and Science, Research and Technology (BMBF)
- <sup>n</sup> supported by the Spanish Ministry of Education and Science through funds provided by CICYT
- <sup>o</sup> supported by the Particle Physics and Astronomy Research Council
- <sup>p</sup> supported by the US Department of Energy
- <sup>q</sup> supported by the US National Science Foundation

# 1 Introduction

Elastic photoproduction of  $\rho^0$  mesons,  $\gamma p \rightarrow \rho^0 p$ , has been studied in fixed target experiments at photon-proton centre-of-mass energies  $W$  up to 20 GeV [1]-[25] and at HERA [26]-[28] for  $W$  up to approximately 200 GeV. In both cases the reaction exhibits the features of a soft diffractive process, namely a weak energy dependence and a differential cross section  $d\sigma/dt \propto \exp(bt)$  at low  $|t|$  values, where  $t$  is the squared four-momentum exchanged between the photon and the proton. These features, typical of elastic hadron-hadron interactions, are consistent with the expectations of the Vector Meson Dominance model (VDM) [29] in which the photon is assumed to fluctuate into a vector meson before scattering from the proton. In elastic  $\rho^0$  photoproduction the photon thus appears to behave like an ordinary hadron which interacts elastically with the proton. Many aspects of  $\rho^0$  photoproduction remain however to be clarified – among them, the  $W$  dependence of the cross section, the origin of the asymmetric  $\rho^0$  resonance shape and the extent to which the helicity of the photon is transferred to the vector meson. Perturbative QCD calculations which have been able to successfully describe the photoproduction of  $J/\psi$  mesons [30] are not strictly applicable to  $\rho^0$  photoproduction at low  $|t|$ . In general, photoproduction of  $\rho^0$  mesons at HERA may offer a means of investigating the nature of soft hadronic interactions as well as the hadronic features of the photon.

Little is known about proton-dissociative  $\rho^0$  production with real photons,  $\gamma p \rightarrow \rho^0 N$ , where  $N$  is a state of mass  $M_N$  into which the proton diffractively dissociates. Data exist for the virtual photon case: the H1 Collaboration at HERA has recently investigated proton-dissociative  $\rho^0$  production for photon virtualities  $Q^2 > 7 \text{ GeV}^2$  [31]. The H1 results indicate that the cross section for this process has the same dependence on  $Q^2$  and  $W$  and the same helicity structure as the elastic reaction. These observations support the hypothesis of factorisation of the diffractive vertex [32], which has been extensively studied in hadron-hadron reactions (see e.g. [32]-[37]). The H1 data also show that the  $t$  distribution is exponential but shallower than that for the elastic case. In photoproduction, proton-dissociative production of  $\rho^0$  mesons can provide yet another way to study diffraction, the hadronic properties of the photon and the nature of soft hadronic processes. In conjunction with the elastic reaction, it can provide a test of factorisation. Moreover, a detailed understanding of proton-diffractive dissociation is mandatory for the study of the elastic reaction, for which it is the main source of background when the scattered proton is not measured.

This paper describes a measurement of  $\rho^0$  photoproduction in the elastic and proton-dissociative reactions. The measurement was performed using data collected in 1994 by the ZEUS experiment at HERA for the processes  $ep \rightarrow e\pi^+\pi^-p$  and  $ep \rightarrow e\pi^+\pi^-N$  at small photon virtualities,  $Q^2 \lesssim 4 \text{ GeV}^2$ . The symbol  $e$  indicates positrons.

For the data presented here the scattered positron was not detected. The scattered proton was measured only for a subsample of the data. In general the relevant kinematic quantities were determined from the measured three-momenta of the two pions from the  $\rho^0$  decay.

With respect to the ZEUS 1993 data [26], the present results on elastic  $\rho^0$  photoproduction feature larger statistics, a wider  $W$  range and smaller systematic uncertainties. Two of the main contributions to the uncertainties of the 1993 results were significantly reduced: the calorimeter trigger efficiency was evaluated directly from the data and the contamination of



proton-dissociative events was determined by using a subsample of the data in which elastic events were unambiguously selected by detecting the final state proton.

The larger statistics and wider kinematic range allowed the study of the  $\pi^+\pi^-$  mass spectrum as a function of  $t$ ,  $W$  and the decay pions' polar and azimuthal angles in the helicity frame. The shape of the  $\pi^+\pi^-$  mass spectrum in the reaction  $ep \rightarrow e\pi^+\pi^-p$  is interesting since, in the framework of the Söding model [38], it depends on the interference between resonant  $\rho^0$  and non-resonant  $\pi^+\pi^-$  production.

The cross section for elastic  $\rho^0$  photoproduction,  $\sigma_{\gamma p \rightarrow \rho^0 p}$ , was extracted as a function of  $W$ . The  $W$  dependence of the cross section, in Regge theory [39], is related to the intercept  $\alpha_P(0)$  of the pomeron trajectory exchanged between the proton and the hadronic fluctuation of the photon.

The differential cross section  $d\sigma/d|t|$  was determined and its shape studied as a function of  $W$ . Regge theory predicts that the slope of the exponential  $t$  distribution becomes increasingly steep with increasing  $W$ ; the rate of change of the  $t$  slope with  $W$ , at high values of  $W$ , is related to the slope of the pomeron trajectory,  $\alpha_P'$ .

The decay pion angular distributions in the helicity frame were studied and the  $\rho^0$  spin density matrix elements  $r_{00}^{04}$ ,  $r_{1-1}^{04}$  and  $\Re[r_{10}^{04}]$  determined. The behaviour of these matrix elements as a function of the two-pion invariant mass  $M_{\pi\pi}$  and of  $W$  was investigated. This made it possible to test the validity of  $s$ -channel helicity conservation (SCHC).

We also present results on  $\rho^0$  photoproduction with diffractive dissociation of the proton in the range  $M_N^2 < 0.1W^2$ . The limit was chosen following refs. [32, 40] and corresponds to the region where diffractive interactions dominate. The distributions of  $M_{\pi\pi}$ ,  $W$ , the polar and azimuthal angles of the pions in the helicity frame and the  $t$  dependence of proton-dissociative  $\rho^0$  photoproduction were studied. The ratio of the cross sections for elastic and proton-dissociative  $\rho^0$  photoproduction was determined.

Finally, we used the data on the reaction  $ep \rightarrow e\pi^+\pi^-p$  to evaluate the pion-proton total cross section in a model dependent way. As mentioned earlier, the shape of the  $\pi^+\pi^-$  mass spectrum is sensitive to the interference between resonant  $\rho^0$  and non-resonant  $\pi^+\pi^-$  production. In the latter case, one (or both) of the pions interacts with the proton. The mass spectrum thus depends on the pion-proton cross section. In the framework of a calculation by Ryskin and Shabelski [41], we determined this cross section at a pion-proton centre-of-mass energy of the order of 50 GeV, beyond the reach of any existing pion beam.

## 2 Experimental set-up

### 2.1 HERA

The data discussed here were collected in 1994 using the HERA collider which operated with 820 GeV protons and 27.5 GeV positrons. The proton and positron beams each contained 153 colliding bunches, together with 17 additional unpaired proton and 15 unpaired positron bunches. These additional bunches were used for background studies.

## 2.2 The ZEUS detector

A detailed description of the ZEUS detector can be found elsewhere [42, 43]. The components which are most relevant for this analysis are briefly discussed below.

Charged particles are tracked by the inner tracking detectors which operate in a magnetic field of 1.43 T provided by a thin superconducting solenoid. Immediately surrounding the beam pipe is the vertex detector (VXD), a drift chamber with 120 radial cells, each with 12 sense wires [44]. It is surrounded by the central tracking detector (CTD), which consists of 72 cylindrical drift chamber layers, organised into 9 superlayers covering the polar angle region<sup>1</sup>  $15^\circ < \theta < 164^\circ$  [45]. The transverse momentum resolution for tracks traversing all superlayers is  $\sigma(p_T)/p_T \simeq \sqrt{(0.005p_T)^2 + (0.016)^2}$ , with  $p_T$  in GeV. The Rear Tracking Detector (RTD) consists of a planar drift chamber with three layers of drift cells with the wires oriented at  $0^\circ$ ,  $+60^\circ$  and  $-60^\circ$  with respect to the horizontal plane; polar angles between  $160^\circ$  and  $170^\circ$  are covered [46].

The high resolution uranium-scintillator calorimeter (CAL) [47] consists of three parts: the forward (FCAL), the barrel (BCAL) and the rear calorimeter (RCAL); they cover the polar angle regions  $2.6^\circ$  to  $36.7^\circ$ ,  $36.7^\circ$  to  $129.1^\circ$ , and  $129.1^\circ$  to  $176.2^\circ$ , respectively. Each part is subdivided transversely into towers. The towers are segmented longitudinally into one electromagnetic section (EMC) and one (in RCAL) or two (in BCAL and FCAL) hadronic sections (HAC). These sections are further subdivided into cells; each cell is viewed by two photomultiplier tubes. The CAL energy resolution, as measured under test beam conditions, is  $\sigma_E/E = 0.18/\sqrt{E}$  for electrons and  $\sigma_E/E = 0.35/\sqrt{E}$  for hadrons ( $E$  in GeV).

The Veto Wall, the C5 counter and the small angle rear tracking detector (SRTD) [48] all consist of scintillation counters and are located at  $Z = -730$  cm,  $Z = -315$  cm and  $Z = -150$  cm, respectively. Particles which are generated by interactions of protons with residual gas molecules in the beam pipe (proton “beam-gas” events) upstream of the nominal  $ep$  interaction point reach the RCAL, the Veto Wall, the SRTD and C5 at different times than particles originating from the nominal  $ep$  interaction point. Proton beam-gas events are thus rejected by timing measurements in these detectors.

The proton remnant tagger (PRT1) [49] is used to tag events in which the proton diffractively dissociates. It consists of two layers of scintillation counters perpendicular to the beam and is positioned at  $Z = 515$  cm. The two layers are separated by a 1 mm thick lead absorber. Each layer is split vertically into two halves and each half is read out by a photomultiplier tube. The counters have an active area of  $30\text{ cm} \times 26\text{ cm}$  with a hole of  $6.0\text{ cm} \times 4.5\text{ cm}$  at the centre to accommodate the HERA beam pipe. The PRT1 covers the range in pseudorapidity ( $\eta = -\ln \tan(\theta/2)$ ) from 4.3 to 5.8.

The Leading Proton Spectrometer (LPS) [28] detects charged particles scattered at small angles and carrying a substantial fraction,  $x_L$ , of the incoming proton momentum; these particles remain in the beam pipe and their trajectory is measured by a system of position sensitive silicon micro-strip detectors very close to the proton beam. The detectors are located in six stations, S1 to S6, placed along the beam line in the direction of the outgoing protons, at

---

<sup>1</sup>The coordinate system used in this paper has the  $Z$  axis pointing in the proton beam direction, hereafter referred to as “forward”, the  $X$  axis pointing horizontally towards the centre of HERA and the  $Y$  axis pointing upwards. The polar angle  $\theta$  is defined with respect to the  $Z$  direction.

$Z = 23.8$  m,  $40.3$  m,  $44.5$  m,  $63.0$  m,  $81.2$  m and  $90.0$  m from the interaction point, respectively. The track deflections induced by the magnets in the proton beam line are used for the momentum analysis of the scattered proton. For the present measurement, only the stations S4, S5 and S6 were used. With this configuration, for  $x_L$  close to unity, a resolution of 0.4% on the longitudinal momentum and 5 MeV on the transverse momentum has been achieved. The transverse momentum resolution is however dominated by the proton beam intrinsic transverse momentum spread at the interaction point of  $\approx 40$  MeV in the horizontal plane and  $\approx 90$  MeV in the vertical plane.

The luminosity was determined from the rate of the Bethe-Heitler process,  $ep \rightarrow e\gamma p$ , where the photon is measured with a calorimeter (LUMI) located at  $Z = -107$  m in the HERA tunnel downstream of the interaction point in the direction of the outgoing positrons [50].

### 3 Kinematics

The reactions under study (cf. Fig. 1) are

$$e(k)p(P) \rightarrow e(k')\rho^0(V)p(P') \text{ and } e(k)p(P) \rightarrow e(k')\rho^0(V)N(N'), \quad (1)$$

where the symbols in parentheses denote the four-momenta of the corresponding particles (or particle system, in the case of  $N$ ).

The kinematics of the inclusive scattering of unpolarised positrons and protons is described by the positron-proton centre-of-mass energy squared,  $s$ , and any two of the following variables:

- $Q^2 = -q^2 = -(k - k')^2$ , the negative square of the exchanged photon's four-momentum.
- $y = (q \cdot P)/(k \cdot P)$ , the fraction of the positron energy transferred to the hadronic final state in the rest frame of the initial state proton.
- $W^2 = (q + P)^2 = -Q^2 + 2y(k \cdot P) + M_p^2 \simeq ys$ , the centre-of-mass energy squared of the photon-proton system, where  $M_p$  is the proton mass.

For the exclusive reaction  $ep \rightarrow e\rho^0 p$  ( $\rho^0 \rightarrow \pi^+\pi^-$ ) and the proton-dissociative process  $ep \rightarrow e\rho^0 N$ , the following additional variables are used:

- $t = (q - V)^2 = (P - P')^2$ , the four-momentum transfer squared at the photon- $\rho^0$  vertex; for the proton-dissociative reaction,  $t = (q - V)^2 = (P - N')^2$ .
- The angle between the  $\rho^0$  production plane (which contains the virtual photon and the  $\rho^0$ ) and the positron scattering plane.
- The polar and azimuthal angles,  $\theta_h$  and  $\varphi_h$ , of the decay  $\pi^+$  in the  $\rho^0$  helicity frame, where the  $\rho^0$  is at rest and the polar angle  $\theta_h$  is defined as the angle between the direction opposite to that of the outgoing proton and the direction of the  $\pi^+$ . The azimuthal angle  $\varphi_h$  is the angle between the decay plane and the  $\rho^0$  production plane.
- $x_L$ , the fraction of the incoming beam momentum carried by the outgoing proton.

- For the proton-dissociative reaction, the mass  $M_N$  of the diffractively produced state  $N$  is relevant. In the present analysis however it was not possible to measure this quantity directly and the  $M_N$  range covered was obtained from Monte Carlo simulations (see section 5.2).

In the present analysis, events were selected in which the final state positron was scattered at an angle too small to be detected in the uranium calorimeter. Thus the angle between the  $\rho^0$  production plane and the positron scattering plane was not measured. In such untagged photoproduction events, the  $Q^2$  value ranges from the kinematic minimum  $Q_{min}^2 = M_e^2 y^2 / (1 - y) \sim 10^{-9} \text{ GeV}^2$ , where  $M_e$  is the electron mass, to the value at which the scattered positron is observed in the uranium calorimeter,  $Q_{max}^2 \approx 4 \text{ GeV}^2$ , with a median  $Q^2$  of approximately  $4 \times 10^{-6} \text{ GeV}^2$ . Since the typical  $Q^2$  is small, the photon-proton centre-of-mass energy can be approximated by

$$W^2 = 4E_p E_e y \simeq 2(E_p - p_{Z\rho}) E_p, \quad (2)$$

where  $E_p$ ,  $E_e$  and  $E_\rho$  are the energies of the incoming proton, of the incoming positron and of the  $\pi^+\pi^-$  system, respectively; the longitudinal momentum of the  $\pi^+\pi^-$  system is denoted by  $p_{Z\rho}$ . Furthermore for  $Q^2 = Q_{min}^2$ ,  $t$  is given by

$$t = (q - V)^2 \simeq -p_{T\rho}^2, \quad (3)$$

where  $p_{T\rho}$  is the momentum of the  $\pi^+\pi^-$  system transverse to the beam axis. Non-zero values of  $Q^2$  cause  $t$  to differ from  $-p_{T\rho}^2$  by less than  $Q^2$ . A multiplicative correction factor determined with the Monte Carlo generators discussed in section 6 was applied to the  $p_{T\rho}^2$  distribution to account for this effect; the correction was obtained by taking the ratio between the  $t$  and  $p_{T\rho}^2$  distributions at the generator level (cf. e.g. [26]). The correction varies from 1.13 at  $p_{T\rho}^2 = 0$  to 0.62 at  $p_{T\rho}^2 = 0.5 \text{ GeV}^2$ . The result thus obtained is consistent with that found by using LPS tagged events [28], for which  $t$  is measured directly.

## 4 Trigger

ZEUS uses a three-level trigger system [42, 43]. For the present data, the trigger selected events from photoproduction of a vector meson decaying into two charged particles without requiring that the scattered positron be detected.

The first-level trigger required an energy deposit of at least 464 MeV in the electromagnetic section of RCAL (excluding the towers immediately around the beam pipe) and at least one track candidate in the CTD. Events with an energy deposit larger than 1250 MeV in the FCAL towers surrounding the beam pipe were rejected in order to suppress proton beam-gas events along with a large fraction of photoproduction events. This cut also removes large- $M_N$  proton-dissociative events.

At the second-level trigger, the background was reduced by using the measured time of the energy deposits and the summed energies from the calorimeter.

The full event information was available at the third-level trigger and a simplified reconstruction procedure was used. Tighter calorimeter timing cuts as well as algorithms to remove cosmic muons were applied. Exactly one reconstructed vertex was demanded, with a  $Z$  coordinate within  $\pm 66 \text{ cm}$  of the nominal interaction point. Furthermore, the events were required to satisfy at least one of the following conditions:

1. less than four reconstructed tracks and at least one pair with invariant mass less than 1.5 GeV (assuming they are pions);
2. less than six reconstructed tracks with a total invariant mass less than 2.5 GeV (again assuming pions).

Both sets of third-level triggers were prescaled by a factor six. An integrated luminosity of  $2.17 \pm 0.03 \text{ pb}^{-1}$  thus yielded approximately 725,000 events.

No requirements were imposed on the LPS or PRT1 at the trigger level.

For the present analysis, unlike what was done in [26, 28], the RCAL trigger efficiency at the first level was determined [51, 52] using the data rather than a Monte Carlo simulation. A sample of two-track events ( $\rho^0$  candidates) was used. Since one of the two pions is sufficient to trigger the event, the efficiency for RCAL to trigger on a charged pion was evaluated as the fraction of events in which the second pion could have satisfied the trigger and in which it actually did. This was feasible since, for a subsample of the events, it was possible to uniquely determine which of the two pions satisfied the RCAL trigger. The results for the efficiency were parametrised as a function of the momentum and polar angle of the pion, separately for positive and negative pions. The efficiency was then applied as a multiplicative weight to each event. Figure 2 shows the efficiency as a function of the momentum. The uncertainty is dominated by statistics. The same parametrisation was also used in [53].

## 5 Event selection

### 5.1 Event selection for elastic $\rho^0$ photoproduction

The following offline requirements were imposed to select candidates for the reaction  $ep \rightarrow e\pi^+\pi^-p$ :

- Exactly two tracks in the CTD from particles of opposite charge, both associated with the reconstructed vertex.
- The coordinates of the reconstructed vertex in the range  $-0.5 < X < 0.8 \text{ cm}$ ,  $-0.8 < Y < 0.5 \text{ cm}$  and  $-29 < Z < 38 \text{ cm}$  (approximately corresponding to three standard deviations of the vertex distribution).
- Transverse momentum greater than 150 MeV and  $|\eta| < 2.1$  for each of the two tracks, thus restricting the data to a region of well understood track reconstruction efficiency.
- Each CAL cell which is more than 40 cm (in the EMC) or 55 cm (in the HAC) away from the extrapolated impact position of either track should not have an energy deposit above a given value. The maximum allowed energy deposits varied from 160 to 240 MeV depending on the calorimeter part and section. This cut rejects events with additional particles, including events with the scattered positron in RCAL.

After applying these requirements, the pion mass was assigned to each track and the analysis was restricted to events reconstructed in the kinematic region defined by:

$$\begin{aligned} 0.55 < M_{\pi\pi} &< 1.2 \text{ GeV}, \\ p_{T\rho}^2 &< 0.5 \text{ GeV}^2, \\ 50 < W &< 100 \text{ GeV}. \end{aligned} \tag{4}$$

The restricted range in the two-pion invariant mass  $M_{\pi\pi}$  reduces the contamination from reactions involving other mesons, in particular from  $\phi$  production with subsequent  $\phi \rightarrow K^+ K^-$  decay and  $\omega \rightarrow \pi^+ \pi^- \pi^0$  production. The requirement on  $p_{T\rho}^2$  limits the background from proton-dissociative  $\rho^0$  production and the selected  $W$  range restricts the data to a region of well understood acceptance. The final sample contains 79,010 events.

## 5.2 Event selection for proton-dissociative $\rho^0$ photoproduction

To select candidates for the reaction  $ep \rightarrow e\pi^+\pi^-N$  all the criteria discussed for the elastic events were applied, except for the cut on the maximum energy deposit in FCAL outside a region around the track impact point. In addition, one of the following three requirements was imposed:

- A signal from the PRT1, tagging particles which originate from proton dissociation. A signal from the PRT1 was defined as a coincidence of signals consistent with that of at least a minimum ionising particle from both scintillator counter layers. In addition the energy deposit in the FCAL towers around the beam pipe was required to be less than 1.2 GeV; this was dictated by the trigger condition discussed above.

This sample contains 2130 events, corresponding to a luminosity of approximately  $0.7 \text{ pb}^{-1}$  for which the PRT1 was operational.

- An energy deposit in the FCAL towers around the beam pipe between 0.4 GeV and 1.2 GeV. The lower limit reduces the contribution from calorimeter noise; the upper one was again a consequence of the trigger condition. Here also the particles from the proton dissociation are tagged.

A total of 945 events was selected.

- A proton measured in the LPS carrying a fraction of the incoming beam momentum  $x_L < 0.98$ . As discussed in [28], the  $x_L$  spectrum measured by the LPS is characterised by a narrow peak at  $x_L \approx 1$  from elastic events and a broad distribution for  $x_L \lesssim 0.98$  ascribed to proton-dissociative events. The cut  $x_L < 0.98$  thus tags the events in which the baryon from the proton dissociation is a proton and rejects elastic events, for which  $x_L$  differs from unity by  $(Q^2 + M_\rho^2 + |t|)/W^2$  [28], i.e. at most 0.2% for photoproduction.

This sample contains 576 events, corresponding to a luminosity of approximately  $0.9 \text{ pb}^{-1}$  for which the LPS was operational [28].

In all cases the  $M_N$  region covered is approximately  $M_N \lesssim 10 \text{ GeV}$ . This limit is set by the requirement at the first-level trigger that less than 1250 MeV be deposited in the FCAL towers around the beam pipe (cf. section 4); since  $M_N$  could not be measured directly, this limit was determined by Monte Carlo studies.

## 6 Monte Carlo generators and acceptance determination

The reaction  $ep \rightarrow e\rho^0 p$  was modelled using the EPSOFT [54] generator, developed in the framework of HERWIG [55]. The generated  $M_{\pi\pi}$ ,  $W$  and  $t$  distributions were reweighted so as to reproduce the measured distributions after reconstruction. Similarly reweighted were the polar and azimuthal angular distributions of the decay pions in the helicity frame. The effective  $W$  dependence of the  $\gamma p$  cross section was taken as  $\sigma \propto W^{0.2}$ . The  $t$  distribution was generated as  $A \exp(-b|t| + ct^2)$  with  $b = 11 \text{ GeV}^{-2}$  and  $c = 4 \text{ GeV}^{-4}$ . The DIPSI [56] generator was used as a cross check of the results obtained with EPSOFT. The LPS acceptance was determined using the average of DIPSI and EPSOFT.

For the simulation of the reaction  $ep \rightarrow e\rho^0 N$ , the EPSOFT Monte Carlo was used (in the case of the PRT1 and FCAL tagged events); for this process, the program is based on the assumption that the cross section for the reaction  $\gamma p \rightarrow \rho^0 N$  is of the form:

$$\frac{d^2\sigma}{dtdM_N^2} = \frac{1}{2} \frac{d\sigma_{\gamma p \rightarrow \rho^0 p}}{dt} \left( \frac{d\sigma_{pp \rightarrow pN}}{dtdM_N^2} / \frac{d\sigma_{pp \rightarrow pp}}{dt} \right), \quad (5)$$

where the ratio  $\frac{d\sigma_{pp \rightarrow pN}}{dtdM_N^2} / \frac{d\sigma_{pp \rightarrow pp}}{dt}$  is obtained from fits to  $pp$  data [54].

As a cross check of the results obtained with EPSOFT, the PYTHIA generator [57] was also used (except for the proton-dissociative LPS tagged events for which the acceptance was determined with PYTHIA while EPSOFT was used as a cross check). A cross section of the form  $d^2\sigma/dtdM_N^2 \propto e^{-b|t|} F_{sd}(M_N)/M_N^2$  is assumed in PYTHIA with  $b = b_0 + 2\alpha_p' \ln(W^2/M_N^2)$ ,  $b_0 = 2.8 \text{ GeV}^{-2}$  and  $\alpha_p' = 0.25 \text{ GeV}^{-2}$ , corresponding to an effective  $b \simeq 5 \text{ GeV}^{-2}$  in the kinematic region for which we present our results. The function  $F_{sd}(M_N)$  enhances the cross section in the low mass resonance region and suppresses the production of very large masses [57]. A fit to the generated  $M_N$  spectrum for  $10 < M_N^2 < 200 \text{ GeV}^2$  with a function of the type  $1/M_N^n$  gives  $n = 2.2$ . The effect of the functions  $F_{sd}(M_N)$  and  $b = b(M_N)$  on the spectrum thus is consistent with the result  $n = 2.24 \pm 0.03$  obtained for the diffractive dissociation of the proton in  $\bar{p}p$  collisions [37].

For both EPSOFT and PYTHIA, the value of  $M_N$  ranged between  $M_p + 2M_\pi$  and a maximum fixed by the condition discussed above,  $M_N^2/W^2 \leq 0.1$  [32, 40]. Although the data extend down to  $M_N = M_p + M_\pi$ , the lack of Monte Carlo events below  $M_p + 2M_\pi$  is not expected to give a significant effect [32]. The shapes of the two-pion invariant mass distribution and the  $\rho^0$  decay angular distributions were assumed to be the same as those of the elastic events; this assumption is supported by the data, as discussed in section 8.1.

The radiation of real photons from the incoming or outgoing positron was not simulated, nor were vacuum polarisation loops in the virtual photon; their effects on the cross section were estimated to be smaller than 2% [58].

The generated events were passed through a detailed simulation of the ZEUS detector and trigger. They were then subjected to the same reconstruction and analysis programs as the data. It was checked that all measured distributions were described well by the simulated events. The acceptance in a given bin was then determined as the ratio of the number of accepted Monte Carlo events to the number generated in the selected kinematic range. The

acceptance, calculated in this manner, accounts for the geometric acceptance, the detector and reconstruction efficiencies, the detector resolution and the trigger efficiency. As explained in section 4 however, the efficiency of the RCAL trigger was evaluated from the data and then applied as a multiplicative weight to each event.

Figure 3 shows the overall acceptance for elastic events as a function of  $M_{\pi\pi}$ ,  $W$ ,  $p_{T\rho}^2$ ,  $\cos\theta_h$  and  $\varphi_h$  obtained using EPSOFT. The average acceptance is 15%. The dip in the acceptance at the  $M_{\pi\pi}$  value corresponding to the  $\rho^0$  peak is a consequence of the mass resolution. The acceptance as a function of  $p_{T\rho}^2$  and  $M_N$ , for proton-dissociative events tagged with the PRT1, is shown in Fig. 4. As for the elastic case, the acceptance is essentially independent of  $p_{T\rho}^2$ . While PYTHIA and EPSOFT give consistent results for the shape of the acceptance for the PRT1 tagged events (and for those tagged in the FCAL or in the LPS with  $x_L < 0.98$ ), the normalisation differs by up to a factor of two.

## 7 Elastic $\rho^0$ photoproduction

### 7.1 Background to elastic $\rho^0$ photoproduction

After the selection cuts described in section 5.1, the main source of background was proton-dissociative events in which the mass  $M_N$  was small and no particle from the system  $N$  was detected.

The fraction of proton-dissociative events in the sample selected with the cuts of section 5.1 was determined as follows. Proton-dissociative events were selected with the PRT1 (or the FCAL, but we shall concentrate on the PRT1 tagged sample in the following) as described in section 5.2. The ratios  $w$  of the uncorrected  $M_{\pi\pi}$ ,  $W$ ,  $\cos\theta_h$  and  $\varphi_h$  distributions for the proton-dissociative sample (selected with the PRT1) and the sample obtained with the elastic cuts (for the period in which the PRT1 was operational) were found consistent with being flat, as shown in Fig. 5. Since according to both PYTHIA and EPSOFT the requirement of activity in the PRT1 (or the FCAL) does not affect the shape of the acceptance, this result indicates that proton-dissociative and elastic  $\rho^0$  photoproduction have the same  $M_{\pi\pi}$ ,  $W$ ,  $\cos\theta_h$  and  $\varphi_h$  distributions. On the contrary, the ratio of the  $p_{T\rho}^2$  distributions, also shown in Fig. 5, rises with  $p_{T\rho}^2$ ; since for both reactions the acceptance has the same shape as a function of  $p_{T\rho}^2$  (cf. Figs. 3 and 4), this indicates a shallower  $p_{T\rho}^2$  dependence for the proton-dissociative events.

The fraction of proton-dissociative events in the total sample was thus taken to depend on  $p_{T\rho}^2$  only. The  $p_{T\rho}^2$  dependence of the background was determined as follows. Let the  $p_{T\rho}^2$  distribution for the proton-dissociative sample be parametrised as  $dN_{diss}/dp_{T\rho}^2 = A_{diss} \exp(-b_{diss}^{pp} p_{T\rho}^2)$  and that for the elastic sample as  $dN_{el}/dp_{T\rho}^2 = A_{el} \exp(-b_{el}^{pp} p_{T\rho}^2)$ . Also, let  $dN_{PRT-tag}/dp_{T\rho}^2$  and  $dN_{el-cuts}/dp_{T\rho}^2$  indicate the measured  $p_{T\rho}^2$  distributions for the proton-dissociative sample selected with the PRT1 and for the sample obtained with the elastic cuts, respectively. Then the ratio  $w(p_{T\rho}^2)$  can be written as:

$$w(p_{T\rho}^2) = \frac{dN_{PRT-tag}/dp_{T\rho}^2}{dN_{el-cuts}/dp_{T\rho}^2}$$



$$\begin{aligned}
&= \frac{\varepsilon_{diss} dN_{diss}/dp_{T\rho}^2}{\varepsilon_{el} dN_{el}/dp_{T\rho}^2 + \varepsilon_{diss}^{el-cuts} dN_{diss}/dp_{T\rho}^2} \\
&= \frac{\varepsilon_{diss}}{\varepsilon_{el}} \frac{dN_{diss}/dp_{T\rho}^2}{dN_{el}/dp_{T\rho}^2 + (\varepsilon_{diss}^{el-cuts}/\varepsilon_{el}) dN_{diss}/dp_{T\rho}^2} \\
&\propto \frac{dN_{diss}/dp_{T\rho}^2}{dN_{el}/dp_{T\rho}^2 + f_{diss} dN_{diss}/dp_{T\rho}^2} \tag{6}
\end{aligned}$$

$$\begin{aligned}
&= \frac{A_{diss} \exp(-b_{diss}^{app} p_{T\rho}^2)}{A_{el} \exp(-b^{app} p_{T\rho}^2) + f_{diss} A_{diss} \exp(-b_{diss}^{app} p_{T\rho}^2)} \\
&= \frac{1/f_{diss}}{(A_{el}/f_{diss} A_{diss}) \exp[-(b^{app} - b_{diss}^{app}) p_{T\rho}^2] + 1}, \tag{7}
\end{aligned}$$

where  $\varepsilon_{diss}$  indicates the acceptance for proton-dissociative events to pass the proton-dissociative cuts of section 5.2,  $\varepsilon_{el}$  indicates the acceptance for elastic events to pass the elastic cuts of section 5.1, and  $\varepsilon_{diss}^{el-cuts}$  indicates the acceptance for proton-dissociative events to pass the elastic cuts. We introduced the proportionality symbol in eq. (6) to account for the  $p_{T\rho}^2$ -independent ratio of the acceptance for the proton-dissociative events tagged by the PRT1 and that for the elastic events satisfying the elastic cuts. The quantity  $f_{diss}$  is the ratio of the acceptance for proton-dissociative events passing the elastic cuts and that for elastic events passing the elastic cuts; this ratio is taken to be  $p_{T\rho}^2$ -independent.

The difference  $(b^{app} - b_{diss}^{app})$  was determined by fitting eq. (7) to the data in the range  $0 < p_{T\rho}^2 < 0.5 \text{ GeV}^2$  and was found to be  $4.8 \pm 1.5 \text{ (stat.)} \pm 0.5 \text{ (syst.) GeV}^{-2}$  for the proton-dissociative events tagged with the PRT1. The result of the fit is shown as the dashed line in Fig. 5. The systematic uncertainty reflects the sensitivity of the result to the limits of the fitted range, with the lower limit varied between  $p_{T\rho}^2 = 0$  and  $0.075 \text{ GeV}^2$  and the upper one between  $0.3$  and  $0.5 \text{ GeV}^2$ . The proton-dissociative events tagged with the FCAL yield  $(b^{app} - b_{diss}^{app}) = 4.1 \pm 2.0 \text{ (stat.) GeV}^{-2}$ .

To determine the normalisation of the proton-dissociative background the following procedure was adopted. As discussed earlier (cf. section 6) the acceptance for the proton-dissociative events depends on the Monte Carlo program; hence the proton-dissociative sample was not used. Instead we used the sample satisfying the elastic cuts and its subsample [28, 51] in which the presence of a high momentum ( $x_L > 0.98$ ) proton in the LPS identified elastic events. The region  $0.075 < p_{T\rho}^2 < 0.5 \text{ GeV}^2$  was used, where the acceptance of the LPS is well understood [28].

The function  $r(p_{T\rho}^2)$  was introduced, defined as the fraction of proton-dissociative events in the elastic sample:

$$r(p_{T\rho}^2) = \frac{dN_{el-cuts}/dp_{T\rho}^2 - dN_{LPS}/dp_{T\rho}^2}{dN_{el-cuts}/dp_{T\rho}^2}, \tag{8}$$

where  $dN_{LPS}/dp_{T\rho}^2$  is the yield, corrected for the LPS acceptance, for the LPS tagged elastic events ( $x_L > 0.98$ ). Using the notation introduced earlier,  $r(p_{T\rho}^2)$  can be rewritten as

$$r(p_{T\rho}^2) = \frac{1}{D \exp[-(b^{app} - b_{diss}^{app}) p_{T\rho}^2] + 1}, \tag{9}$$

where  $(b^{app} - b_{diss}^{app})$  was taken to be  $4.8 \pm 1.5$  (stat.)  $\pm 0.5$  (syst.)  $\text{GeV}^{-2}$ , as discussed above, and a fit to the data gave  $D = 7.3_{-0.9}^{+1.2}$  (stat.)  $_{-2.1}^{+3.2}$  (syst.). In order to correct for the proton-dissociative background each event was then weighted by  $[1 - r(p_{T\rho}^2)]$ . The resulting integrated fraction of proton-dissociative background in the untagged sample is  $R_{diss} = (20 \pm 2$  (stat.)  $_{-5}^{+6}$  (syst.))% for  $p_{T\rho}^2 < 0.5 \text{ GeV}^2$ .

In summary, function (7) was fitted to proton-dissociative events tagged with the PRT1 to determine  $(b^{app} - b_{diss}^{app})$ . The latter was then used in function (9), which was evaluated using the yields for purely elastic events tagged by the LPS ( $x_L > 0.98$ ) and for the events passing the elastic cuts. The fit result was used to evaluate the normalisation of the proton-dissociative contamination in the sample selected with the elastic cuts and hence the overall contamination  $R_{diss}$ .

Positron beam-gas and proton beam-gas contaminations were estimated from the unpaired bunch event samples to which the selection criteria described earlier were applied. The number of events passing the cuts was then scaled by the ratio between the positron (proton) current in the paired bunches and the current in the positron (proton) unpaired bunches. The contamination due to positron-gas interactions was estimated to be  $(0.6 \pm 0.1)\%$ , while that due to proton-gas events was found to be  $\lesssim (0.01 \pm 0.01)\%$ . The contamination from elastic production of  $\omega$  and  $\phi$  mesons (decaying to  $\pi^+\pi^-\pi^0$ ) was estimated by using simulated events and found to be  $\lesssim 0.5\%$  [51].

All subsequent results are shown after subtraction of the contributions from proton-dissociative events, beam-gas interactions,  $\omega$  and  $\phi$  production.

## 7.2 Results for elastic $\rho^0$ photoproduction

### 7.2.1 Cross section determination

The differential and integrated photoproduction cross sections for the process  $\gamma p \rightarrow \pi^+\pi^-p$  were obtained from the event yield measured for the reaction  $ep \rightarrow e\pi^+\pi^-p$ . The cross sections for these two processes are related by

$$\begin{aligned} \frac{d^2\sigma_{ep \rightarrow e\pi^+\pi^-p}}{dydQ^2} &= \frac{\alpha}{2\pi Q^2} \left[ \left( \frac{1 + (1-y)^2}{y} - \frac{2(1-y)}{y} \cdot \frac{Q_{\min}^2}{Q^2} \right) \cdot \sigma_T^{\gamma^*p \rightarrow \pi^+\pi^-p}(W, Q^2) \right. \\ &\quad \left. + \frac{2(1-y)}{y} \cdot \sigma_L^{\gamma^*p \rightarrow \pi^+\pi^-p}(W, Q^2) \right], \end{aligned} \quad (10)$$

where  $\alpha$  is the fine structure constant and  $\sigma_T^{\gamma^*p \rightarrow \pi^+\pi^-p}(W, Q^2)$  and  $\sigma_L^{\gamma^*p \rightarrow \pi^+\pi^-p}(W, Q^2)$  are the cross sections for transversely and longitudinally polarised virtual photons, respectively. These cross sections are assumed to be

$$\sigma_T^{\gamma^*p \rightarrow \pi^+\pi^-p}(W, Q^2) = \sigma_{\gamma p \rightarrow \pi^+\pi^-p}(W) \left/ \left( 1 + \frac{Q^2}{M_\rho^2} \right)^2 \right., \quad (11)$$

for transversely polarised photons and

$$\sigma_L^{\gamma^* p \rightarrow \pi^+ \pi^- p}(W, Q^2) = \sigma_T^{\gamma^* p \rightarrow \pi^+ \pi^- p}(W, Q^2) \cdot \frac{Q^2}{M_\rho^2} \xi^2 \quad (12)$$

for longitudinally polarised photons, where  $\xi$  is a proportionality constant of order unity (cf. e.g. [1]). The results presented in this paper are insensitive to the value of  $\xi^2$ : varying  $\xi^2$  between 0 and 1 has negligible effects.

Substituting the latter two expressions into equation (10) yields:

$$\frac{d^2 \sigma_{ep \rightarrow e \pi^+ \pi^- p}}{dy dQ^2} = \varphi(y, Q^2) \cdot \sigma_{\gamma p \rightarrow \pi^+ \pi^- p}(W(y)), \quad (13)$$

which defines the effective photon flux  $\varphi(y, Q^2)$ .

From eq. (13), knowing the effective photon flux, it was then possible to determine the cross section  $\sigma_{\gamma p \rightarrow \pi^+ \pi^- p}$ . As an example, the differential cross section  $d\sigma_{\gamma p \rightarrow \pi^+ \pi^- p}/dM_{\pi\pi}$  was evaluated in each  $M_{\pi\pi}$  bin of width  $\Delta M_{\pi\pi}$  as

$$\frac{d\sigma_{\gamma p \rightarrow \pi^+ \pi^- p}}{dM_{\pi\pi}} = \frac{N_{\pi^+ \pi^-}}{A \cdot L \cdot \Phi \cdot \Delta M_{\pi\pi}}, \quad (14)$$

where  $N_{\pi^+ \pi^-}$  is the number of observed events in the bin after background subtraction and correction for the RCAL trigger efficiency,  $L$  the integrated luminosity and  $A$  the overall acceptance in the bin excluding the RCAL efficiency. The integral of the effective photon flux  $\varphi(y, Q^2)$  over the  $y$  and  $Q^2$  ranges covered by the experiment is indicated as  $\Phi$ . In the following, for brevity, the subscript  $\gamma p \rightarrow \pi^+ \pi^- p$  will be dropped.

### 7.2.2 Differential cross section $d\sigma/dM_{\pi\pi}$ for the reaction $\gamma p \rightarrow \pi^+ \pi^- p$

In Fig. 6 the differential cross section  $d\sigma/dM_{\pi\pi}$  for the process  $\gamma p \rightarrow \pi^+ \pi^- p$  is shown in the kinematic range  $|t| < 0.5 \text{ GeV}^2$  and  $50 < W < 100 \text{ GeV}$ . Figure 7 shows  $d\sigma/dM_{\pi\pi}$  for different  $t$  bins. The  $\rho^0$  resonance shape is skewed, as observed in previous measurements [1]-[28]. This can be understood in terms of the interference between resonant  $\rho^0$  production and non-resonant  $\pi^+ \pi^-$  production [38, 41].

Fits to the points of Fig. 6 were performed in the range  $0.55 < M_{\pi\pi} < 1.2 \text{ GeV}$  with the following parametrisation [26]:

$$\frac{d\sigma}{dM_{\pi\pi}} = \left| A \frac{\sqrt{M_{\pi\pi} M_\rho \Gamma_\rho}}{M_{\pi\pi}^2 - M_\rho^2 + i M_\rho \Gamma_\rho} + B \right|^2 + f_{PS}, \quad (15)$$

where  $M_\rho$  is the nominal  $\rho^0$  mass and  $\Gamma_\rho = \Gamma_0(p^*/p_0^*)^3(M_\rho/M_{\pi\pi})$  the momentum dependent  $\rho^0$  width, with  $\Gamma_0$  the  $\rho^0$  width,  $p^*$  the  $\pi$  momentum in the  $\pi\pi$  rest frame and  $p_0^*$  the value of  $p^*$

Parameter	value	stat. error
$M_\rho$	0.770 GeV	0.002 GeV
$\Gamma_0$	0.146 GeV	0.003 GeV
$A$	$-2.75 \mu\text{b}^{1/2}$	$0.04 \mu\text{b}^{1/2}$
$B$	$1.84 \mu\text{b}^{1/2} \text{ GeV}^{-1/2}$	$0.06 \mu\text{b}^{1/2} \text{ GeV}^{-1/2}$
$A_{PS}$	$0.030 \mu\text{b}/\text{GeV}$	$0.015 \mu\text{b}/\text{GeV}$

Table 1: Results of the fit to the mass spectrum of Fig. 6 for  $50 < W < 100$  GeV and  $|t| < 0.5 \text{ GeV}^2$  using expression (15). Only statistical errors are given.

at the  $\rho^0$  nominal mass. The non-resonant amplitude is denoted by  $B$  and is assumed to be constant and real. The term  $f_{PS}$  is a first order polynomial of the form  $f_{PS} = A_{PS}(1 + B_{PS}M_{\pi\pi})$  accounting for residual background from the process  $\gamma p \rightarrow Xp$ . The coefficient  $B_{PS}$  was estimated to be  $B_{PS} = 1.5 \text{ GeV}^{-1}$  from Monte Carlo studies in which PYTHIA [57] was used to simulate the reaction  $ep \rightarrow eXp$ . The fitted value of  $A_{PS}$  corresponds to an integrated contribution typically smaller than 1% of the total, independent of  $W$  and  $p_T^2$ . Table 1 gives the parameters of the fit for the spectrum shown in Fig. 6. The fitted values of the  $\rho^0$  mass and width are consistent with the Particle Data Group tables [59] and the  $\chi^2/ndf$  for the fit is 15.3/21.

The fits to  $d\sigma/dM_{\pi\pi}$  were repeated in a different way. The mass spectrum was corrected for the acceptance excluding the effects of migration. The mass spectrum was then fitted with formula (15) convoluted with a Gaussian which describes the detector resolution. The width of the Gaussian varied between 6 and 14 MeV depending on  $W$ . The resulting values for the  $\rho^0$  mass and width were  $771 \pm 2 \text{ MeV}$  and  $159 \pm 3 \text{ MeV}$ . The difference between this value of the width and that given in Table 1 gives an indication of the systematic errors associated to the fit. The other parameters of the fit were found to be  $A = -2.75 \pm 0.04 \mu\text{b}^{1/2}$ ,  $B = 1.94 \pm 0.07 \mu\text{b}^{1/2} \text{ GeV}^{-1/2}$  and  $A_{PS} = 0.000 \pm 0.015 \mu\text{b}/\text{GeV}$ . The results for the cross section do not change if this method is used. A fit including a  $\rho^0$ - $\omega$  interference term was also performed [51]; this led to a slightly better  $\chi^2$ . However, none of the results presented in the following changes if such a fit is used.

The curves shown in Fig. 7 were obtained using a calculation [41] based on Söding's model [38]. In this case the mass and the width of the  $\rho^0$  were fixed to the values given in the Particle Data Group tables [59]. The  $\pi$ - $p$  total cross section, a free parameter of model [41], was fitted. This fit is discussed in detail in section 9; here we only remark that the results of the calculation are in good agreement with the data with an average  $\chi^2/ndf$  of 1.0. The non-resonant and interference terms are also shown in the figure; the non-resonant contribution varies very little with  $M_{\pi\pi}$ , a result consistent with the ansatz, made above, that  $B$  is a constant, as assumed in our previous analyses [26, 28].

Fits to the data of Fig. 7 using formula (15) were also carried out, with the mass and the width of the  $\rho^0$  fixed to the values given in table 1. The results for  $|B/A|$  from these fits are shown as a function of  $|t|$  in the upper plot of Fig. 8:  $|B/A|$  decreases with increasing  $|t|$ . The quantity  $|B/A|$  is a measure of the ratio of the non-resonant to resonant contributions;

its decrease with increasing  $|t|$  was already observed in fixed target experiments [1] and can be described in the framework of the Söding model [38, 41].

Alternatively, the following phenomenological parametrisation proposed by Ross and Stodolsky [60] was used to fit the mass distribution:

$$\frac{d\sigma}{dM_{\pi\pi}} = f_\rho \cdot BW_\rho(M_{\pi\pi}) \cdot (M_\rho/M_{\pi\pi})^k + f_{PS}, \quad (16)$$

where  $BW_\rho(M_{\pi\pi})$  is a relativistic  $p$ -wave Breit-Wigner function and the factor  $(M_\rho/M_{\pi\pi})^k$  accounts for the skewing of the signal. In this case the fitted values of the  $\rho^0$  mass and width are  $771 \pm 2$  MeV and  $138 \pm 3$  MeV, respectively; the parameter  $k$  is  $5.13 \pm 0.13$ . Here again the fits were repeated in different  $|t|$  bins, keeping the mass and the width of the  $\rho^0$  fixed to the values just quoted. The parameter  $k$  is plotted as a function of  $|t|$  in the lower part of Fig. 8. The decrease of the amount of skewing with increasing  $|t|$  is, in this case, reflected in the decrease of  $k$ . Our results are in agreement with those found in fixed target photoproduction experiments [18, 19], indicating that skewing of the  $\rho^0$  resonant shape depends only weakly, if at all, on  $W$ . Note that in all  $t$  bins the median  $Q^2$  is lower than  $10^{-5}$  GeV<sup>2</sup>. The results are consistent with the effective expectation of the Söding model [38, 41], as the continuous line in the lower plot of Fig. 8 shows (cf. section 9).

Fits using formula (15) were also performed in bins of  $W$ ,  $\cos\theta_h$  and  $\varphi_h$ , again with the mass and the width of the  $\rho^0$  fixed to the values given in table 1. The ratios  $|B/A|$  from these fits are shown in Fig. 9;  $|B/A|$  appears to be independent of  $W$  (as already suggested by the comparison with the fixed target data, cf. Fig. 8) as well as of the decay pion polar and azimuthal angles in the helicity frame.

### 7.2.3 Integrated $\gamma p \rightarrow \rho^0 p$ cross section

The integrated  $\gamma p \rightarrow \rho^0 p$  cross section for  $|t| < 0.5$  GeV<sup>2</sup> was determined in four  $W$  bins. In each of these bins fits to the mass spectra were performed using equation (15);  $M_\rho$ ,  $\Gamma_0$  and  $B/A$  were fixed to the values given in table 1. Following refs. [26, 27], the cross section was calculated by integrating the resonant contribution obtained from the fit over the range  $2M_\pi < M_{\pi\pi} < M_\rho + 5\Gamma_0$ . Figure 10 and Table 2 show the results. Table 3 gives the results for the reaction  $\gamma p \rightarrow \pi^+\pi^-p$  over the same mass range; it was obtained by integrating the result for the first term in eq. (16).

The systematic uncertainties are dominated by the uncertainties on the acceptance (4-10%), the proton-dissociative background (8.5%) and the number of  $\rho^0$  signal events, which depends on the functional form chosen [51] to fit the mass spectrum (4%); the parameters  $M_\rho$ ,  $\Gamma_0$  and  $B/A$  were also varied within their statistical errors (1.5%). The uncertainty on the acceptance (4-10%) is  $W$  dependent and has two main contributions: the calorimeter trigger efficiency near the threshold (4-10%) and the sensitivity of the results to the cuts (4-2%).

Table 4 summarises the contributions to the systematic uncertainty. The total systematic uncertainty was obtained by summing all contributions in quadrature.

Figure 10 includes a partial compilation of low energy measurements, as well as the recent ZEUS [26] and H1 [27] results. Also shown are parametrisations [52] based on Regge theory

$\langle W \rangle$ [GeV]	$\sigma_{\gamma p \rightarrow \rho^0 p}$ [ $\mu\text{b}$ ]
55	$10.9 \pm 0.2$ (stat.) $^{+1.5}_{-1.3}$ (syst.)
65	$10.8 \pm 0.2$ (stat.) $^{+1.3}_{-1.1}$ (syst.)
75	$11.4 \pm 0.3$ (stat.) $^{+1.0}_{-1.2}$ (syst.)
90	$11.7 \pm 0.3$ (stat.) $^{+1.1}_{-1.3}$ (syst.)

Table 2: Elastic  $\rho^0$  photoproduction cross section for  $|t| < 0.5 \text{ GeV}^2$ , integrated over the mass range  $2M_\pi < M_{\pi\pi} < M_\rho + 5\Gamma_0$  in four  $W$  bins. The results were calculated by integrating the resonant contribution obtained from the fit with eq. (15).

$\langle W \rangle$ [GeV]	$\sigma_{\gamma p \rightarrow \pi^+ \pi^- p}$ [ $\mu\text{b}$ ]
55	$12.2 \pm 0.2$ (stat.) $^{+1.6}_{-1.4}$ (syst.)
65	$12.1 \pm 0.2$ (stat.) $^{+1.2}_{-1.2}$ (syst.)
75	$12.8 \pm 0.3$ (stat.) $^{+1.1}_{-1.3}$ (syst.)
90	$13.1 \pm 0.3$ (stat.) $^{+1.2}_{-1.5}$ (syst.)

Table 3: Elastic  $\pi^+ \pi^-$  photoproduction cross section for  $|t| < 0.5 \text{ GeV}^2$ , integrated over the mass range  $2M_\pi < M_{\pi\pi} < M_\rho + 5\Gamma_0$  in four  $W$  bins. The results were obtained by integrating the first term in eq. (16).

which assume the value of the pomeron intercept found by Donnachie and Landshoff [61] and by Cudell et al. [62], respectively. The  $W$  dependence of the data is described satisfactorily by both.

A least squares fit to the present data alone with a function of the type  $\sigma_{\gamma p \rightarrow \rho^0 p}(W) = \sigma_{\gamma p \rightarrow \rho^0 p}(W_0)(W/W_0)^a$  gives  $\sigma_{\gamma p \rightarrow \rho^0 p}(W_0) = 11.2 \pm 0.1$  (stat.) $^{+1.1}_{-1.2}$  (syst.)  $\mu\text{b}$  at  $W_0 = 71.7 \text{ GeV}$  and  $a = 0.16 \pm 0.06$  (stat.) $^{+0.11}_{-0.15}$  (syst.). The value of  $a$  is consistent with the value expected for a “soft” pomeron,  $a \simeq 0.22$  (see e.g. [61]). The systematic uncertainties were determined by repeating the fit to the cross section obtained after each systematic check. The differences between the values of  $\sigma_{\gamma p \rightarrow \rho^0 p}(W_0)$  and  $a$  thus found and the nominal value were added in quadrature. The dominant contribution to the systematic uncertainty on  $a$  is that due to the trigger efficiency since its effect in different  $W$  bins is not correlated; conversely, the effects of the uncertainty of the proton-dissociative background contamination and that of the procedure to extract the resonant part of the cross section are the same in all  $W$  bins.

#### 7.2.4 Differential cross section $d\sigma/d|t|$

Figure 11a shows the differential cross section  $d\sigma/d|t|$  for the process  $\gamma p \rightarrow \pi^+ \pi^- p$  in the kinematic range  $0.55 < M_{\pi\pi} < 1.2 \text{ GeV}$  and  $50 < W < 100 \text{ GeV}$ . The cross section exhibits the exponential fall characteristic of diffractive processes. A fit to the form

$$\frac{d\sigma}{d|t|} = A_{\pi\pi} e^{-b_{\pi\pi}|t| + c_{\pi\pi}t^2} \quad (17)$$

Contribution from	Uncertainty
Luminosity	1.5%
Acceptance: trigger efficiency	4-10%
Acceptance: sensitivity to cuts	4-2%
$p$ -dissociative background subtraction	8.5%
Background due to elastic $\omega$ and $\phi$ production	1%
Procedure to extract the resonant part of the cross section	4.5%
Radiative corrections	2%
Total	11-14%

Table 4: Individual and total contributions to the systematic uncertainty on the integrated cross section.

was performed. The fitted values of  $b_{\pi\pi}$  and  $c_{\pi\pi}$  are  $11.4 \pm 0.3$  (stat.)  $^{+0.3}_{-0.5}$  (syst.)  $\text{GeV}^{-2}$  and  $2.8 \pm 0.7$  (stat.)  $^{+1.2}_{-1.8}$  (syst.)  $\text{GeV}^{-4}$ , respectively. The main contribution to the systematic errors is the uncertainty of the acceptance.

In Fig. 12 the slope  $b_{\pi\pi}$  resulting from a fit of equation (17) in different mass bins is shown; in this case  $c_{\pi\pi}$  was kept fixed at the value  $2.8 \text{ GeV}^{-4}$ . The rapid decrease of  $b_{\pi\pi}$  with increasing mass is consistent with the results of earlier measurements (cf. e.g. [1]) and effectively is expected in the Söding model [38, 41] as the continuous curve in Fig. 12 shows. The way the curve was obtained is discussed in section 9.

In order to determine  $d\sigma/d|t|$  for the resonant process  $\gamma p \rightarrow \rho^0 p$ , the mass fits with eq. (15) were carried out in each  $|t|$  bin (with  $M_\rho$  and  $\Gamma_0$  fixed to the values of table 1) and the resonant part of the cross section extracted as a function of  $|t|$  and integrated over the range  $2M_\pi < M_{\pi\pi} < M_\rho + 5\Gamma_0$ . The cross section  $d\sigma/d|t|$  thus obtained is plotted in Fig. 11b, where the result of the fit with the function

$$\frac{d\sigma}{d|t|} = A_\rho e^{-b_\rho|t|+c_\rho t^2} \quad (18)$$

is also shown. The parameters of the fit are  $b_\rho = 10.9 \pm 0.3$  (stat.)  $^{+1.0}_{-0.5}$  (syst.)  $\text{GeV}^{-2}$  and  $c_\rho = 2.7 \pm 0.9$  (stat.)  $^{+1.9}_{-1.7}$  (syst.)  $\text{GeV}^{-4}$ . The larger systematic uncertainty of  $b_\rho$  with respect to that of  $b_{\pi\pi}$  reflects the sensitivity to the procedure used to extract the resonant part of the cross section.

Finally the  $|t|$  distribution was studied in three different  $W$  bins; the parameter  $c_\rho$  was fixed to  $2.7 \text{ GeV}^{-4}$ . Table 5 and Fig. 13 show the values of the slope  $b_\rho$  as a function of  $W$  together with the other recent results from HERA [26, 27, 28] and a partial compilation of low energy data [25, 5, 14, 19, 17] (cf. Fig. 9 of ref. [26]).

A fit of the form  $b_\rho(W) = b_\rho(W_0) + 2\alpha_{\rho'} \ln(W/W_0)^2$ , with  $W_0 = 71.7 \text{ GeV}$ , to the present data alone yields  $\alpha_{\rho'} = 0.23 \pm 0.15$  (stat.)  $^{+0.10}_{-0.07}$  (syst.)  $\text{GeV}^{-2}$ . The systematic uncertainty was determined by repeating the fit to the  $b$  values as modified by the effect of each individual

$\langle W \rangle$ [GeV]	$b_\rho$ [GeV <sup>-2</sup> ]
55	$10.6 \pm 0.2$ (stat.) $^{+1.0}_{-0.4}$ (syst.)
65	$11.0 \pm 0.2$ (stat.) $^{+1.0}_{-0.5}$ (syst.)
84	$11.1 \pm 0.1$ (stat.) $^{+1.0}_{-0.6}$ (syst.)

Table 5:  $b_\rho$  as a function of  $W$ .

systematic uncertainty; the differences between the values of  $\alpha_p'$  thus found and the nominal value were added in quadrature. The present result is consistent with  $\alpha_p' = 0.25$  GeV<sup>-2</sup> obtained from fits to data on soft hadronic processes [61]. Such a dependence of  $b_\rho$  on  $W$  is expected to be valid for  $W \gtrsim 5$ -10 GeV [61].

### 7.2.5 Decay angular distributions

The angular distributions of the decay pions allow one to determine the  $\rho^0$  spin density matrix elements. They were determined in the helicity frame, where the dependence on  $\theta_h$  and  $\varphi_h$  can be written as [63]:

$$\frac{1}{\sigma} \frac{d\sigma}{d\cos\theta_h d\varphi_h} = \frac{3}{4\pi} \left[ \frac{1}{2} (1 - r_{00}^{04}) + \frac{1}{2} (3r_{00}^{04} - 1) \cos^2\theta_h - \sqrt{2} \Re[r_{10}^{04}] \sin 2\theta_h \cos\varphi_h - r_{1-1}^{04} \sin^2\theta_h \cos 2\varphi_h \right], \quad (19)$$

with  $r_{00}^{04}$ ,  $r_{10}^{04}$  and  $r_{1-1}^{04}$  the  $\rho^0$  spin density matrix elements. The element  $r_{00}^{04}$  represents the probability that the produced  $\rho^0$  meson has helicity 0;  $r_{1-1}^{04}$  is related to the size of the interference between the helicity non-flip and double flip amplitudes, while  $\Re[r_{10}^{04}]$  is related to the interference between the helicity non-flip and single flip amplitudes. If  $s$ -channel helicity conservation (SCHC) holds,  $r_{1-1}^{04}$  and  $\Re[r_{10}^{04}]$  should be zero;  $r_{00}^{04}$  should also be small because in the kinematic range of the present data the incoming photons are mostly transverse.

Figure 14 shows the acceptance corrected  $\theta_h$  and  $\varphi_h$  distributions for the process  $\gamma p \rightarrow \pi^+ \pi^- p$ . As discussed above (cf. Fig. 5), their shape is consistent with being the same for elastic and proton-dissociative events.

A two-dimensional least-squares fit of equation (19) to the acceptance corrected  $\cos\theta_h$  and  $\varphi_h$  distributions yields  $r_{00}^{04} = 0.01 \pm 0.01$  (stat.)  $\pm 0.02$  (syst.),  $r_{1-1}^{04} = -0.01 \pm 0.01$  (stat.)  $\pm 0.01$  (syst.) and  $\Re[r_{10}^{04}] = 0.01 \pm 0.01$  (stat.)  $\pm 0.01$  (syst.). The result of the fit is shown in Fig. 14. The  $\chi^2/n_{df}$  of the fit is 225/215. A moment analysis gives similar values. The systematic uncertainties are dominated by the error of the acceptance. The two-dimensional  $\theta_h$ ,  $\varphi_h$  distribution was not corrected for the non-resonant and interference contributions, which however appear to have the same  $\cos\theta_h$  and  $\varphi_h$  dependence as the resonant process (cf. Fig. 9).

The present results indicate that in the kinematic range studied the  $\rho^0$  mesons are produced predominantly with helicity  $\pm 1$ . In addition our data are consistent with  $s$ -channel helicity conservation.



The two-dimensional fit described above was repeated in different  $M_{\pi\pi}$  and  $W$  bins. The results found for  $r_{00}^{04}$ ,  $\Re[r_{10}^{04}]$  and  $r_{1-1}^{04}$  are plotted as a function of  $M_{\pi\pi}$  in Fig. 15; the data do not indicate any dependence on  $M_{\pi\pi}$ . It should be noted that in some models (see e.g. [64]), for finite values of  $Q^2$  ( $Q^2 \gtrsim 1 \text{ GeV}^2$ ),  $r_{00}^{04}$  is expected to vary with  $M_{\pi\pi}$ . A variation at large values of  $M_{\pi\pi}$ ,  $M_{\pi\pi} \gtrsim 0.9$ , was observed in fixed target photoproduction experiments [18]. The results are also independent of  $W$  as shown in Fig. 16; for this study the  $W$  range was restricted to  $W < 80 \text{ GeV}$  since at large  $W$  the two-dimensional acceptance in the  $\cos\theta_h, \varphi_h$  plane is rapidly varying. Here again, the comparison of these results with those obtained for  $r_{1-1}^{04}$  and  $\Re[r_{10}^{04}]$  by the low energy experiments (cf. e.g. [17]) confirms the lack of  $W$  dependence for these elements. Further investigations, not presented here, show that if SCHC and natural parity exchange in the  $t$ -channel are assumed, then  $r_{00}^{04}$ ,  $\Re[r_{10}^{04}]$  and  $r_{1-1}^{04}$  appear independent also of  $t$ , in the  $t$  range studied here [51].

## 8 Proton-dissociative $\rho^0$ photoproduction

### 8.1 $M_{\pi\pi}$ , $W$ , $\cos\theta_h$ , $\varphi_h$ distributions

As discussed earlier (section 7.1), proton-dissociative events selected with the PRT1 or the FCAL as described in section 5.2 have the same  $M_{\pi\pi}$ ,  $W$ ,  $\cos\theta_h$  and  $\varphi_h$  dependence as the elastic events selected by the cuts of section 5.1 (which contain only a contamination  $R_{diss} = 20\%$  from proton-dissociative events). This was deduced from the fact that the ratios of the uncorrected  $M_{\pi\pi}$ ,  $W$ ,  $\cos\theta_h$  and  $\varphi_h$  distributions for the proton-dissociative sample and the sample obtained with the elastic cuts are consistent with being flat, as Fig. 5 shows.

This result supports the hypothesis of factorisation of the diffractive vertices. As discussed in [32], given the dissociative reaction  $ha \rightarrow Na$  and the elastic one  $ha \rightarrow ha$ , with  $h$  and  $a$  hadrons, factorisation implies

$$\frac{d^2\sigma_{diss}/dtd(M_N^2/s_{ha})}{d^2\sigma_{el}/dt} = f(s, M_N^2/s_{ha}, t), \quad (20)$$

i.e. at given  $s_{ha}$ ,  $M_N^2$  and  $t$ , the ratio of the diffractive dissociation cross section to the elastic cross section is a constant independent of hadron  $a$ ; here  $s_{ha}$  indicates the square of the centre-of-mass energy of the  $ha$  system.

The results presented in sections 8.2 and 8.3 were obtained for the production of pion pairs in the range  $0.55 < M_{\pi\pi} < 1.2 \text{ GeV}$  and not for the resonant process. This was done because of the limited statistics.

### 8.2 $|t|$ distribution

As discussed in section 7.1, the  $p_{T\rho}^2$  and hence the  $|t|$  distribution for proton-dissociative events is shallower than for elastic events. The acceptance corrected  $|t|$  distribution for the reaction  $\gamma p \rightarrow \pi^+\pi^-N$  obtained with the PRT1 tagged events is shown in Fig. 17 (solid symbols).

The continuous line represents the result of a fit with an exponential function of the form  $Ae^{-b_{diss}|t|}$  in the range  $0.025 < |t| < 0.5 \text{ GeV}^2$  and corresponds to a  $t$ -slope  $b_{diss} = 5.8 \pm 0.3 \text{ (stat.)} \pm 0.5 \text{ (syst.) GeV}^{-2}$  for the kinematic range  $50 < W < 100 \text{ GeV}$  and  $(M_p + M_\pi)^2 < M_N^2 < 0.1W^2$ ; the upper limit of  $M_N$  ( $M_{N_{\max}} = \sqrt{0.1W_{\max}^2} \approx 30 \text{ GeV}$ ) was chosen following refs. [40, 32] and corresponds to the region where diffractive interactions dominate. A fit with a function of the form  $A \exp(-b'_{diss}|t| + c'_{diss}t^2)$  gives  $b'_{diss} = 6.6 \pm 1.1 \text{ (stat.) GeV}^{-2}$  and  $c'_{diss} = 1.8 \pm 2.4 \text{ (stat.) GeV}^{-4}$ . If the analysis is repeated for  $(M_p + M_\pi)^2 < M_N^2 < 100 \text{ GeV}^2$ , which is the region covered by the data, the  $t$ -slope for a single exponential is  $6.4 \pm 0.3 \text{ (stat.)} \pm 0.6 \text{ (syst.) GeV}^{-2}$ . The dip at low  $|t|$  is a consequence of  $t_{\min}$  being non-zero at large values of  $M_N$  ( $|t_{\min}| \approx 0.006 \text{ GeV}^{-2}$  for  $M_N = 0.1W^2$ ); it disappears for  $M_N^2 < 100 \text{ GeV}^2$ .

In Fig. 17 the open circles show the distribution for the LPS tagged events in the kinematic range  $50 < W < 100 \text{ GeV}$  and  $(M_p + M_\pi)^2 < M_N^2 < 0.1W^2$ . A fit of an exponential function to these points yields a slope of  $5.8 \pm 0.5 \text{ (stat.)} \pm 0.9 \text{ (syst.) GeV}^{-2}$ , in agreement with the result found with the PRT1 tagged events.

As mentioned earlier, the  $t$  distribution determined both for the PRT1 and the LPS tagged events is for  $\gamma p \rightarrow \pi^+\pi^-N$ , not for the resonant process  $\gamma p \rightarrow \rho^0 N$ . From the elastic data however one finds that the difference of the  $t$ -slopes for the reaction  $\gamma p \rightarrow \pi^+\pi^-p$  and for  $\gamma p \rightarrow \rho^0 p$  is  $\simeq 0.5 \text{ GeV}^{-2}$ .

For the result obtained with the PRT1 tagged events, the systematic error includes the difference of the result obtained with the PRT1 and the FCAL tagged events, as well as the sensitivity to the Monte Carlo model used (EPSOFT vs PYTHIA) and to the shape of the generated  $d\sigma/dM_N^2 \propto (1/M_N)^n$  spectrum ( $n$  was varied in the range  $2.0 < n < 2.4$ ). For the result obtained with the LPS tagged events, the sensitivity to the selection cuts and the fitted  $|t|$  range was also included.

The  $t$ -slope in proton-dissociative  $\rho^0$  photoproduction is thus smaller than that for the elastic process by about  $5 \text{ GeV}^{-2}$ . This is consistent with the results found for virtual photons [31] and with those obtained for hadron-hadron collisions [32]-[37]; it is also in agreement with theoretical estimates (cf. e.g. [65]).

### 8.3 Ratio of the elastic to the proton-dissociative $\rho^0$ photoproduction cross sections

Because of the large discrepancy in the normalisation of the acceptance obtained with PYTHIA and EPSOFT for proton-dissociative events, the cross section for the process  $\gamma p \rightarrow \rho^0 N$  was not determined directly from the PRT1, FCAL or low  $x_L$  LPS tagged events. We instead determined the ratio of the elastic to the proton-dissociative  $\rho^0$  photoproduction cross sections,  $\sigma_{\gamma p \rightarrow \rho^0 p} / \sigma_{\gamma p \rightarrow \rho^0 N}$ , using the ratio  $R_{diss}$  found by means of the LPS tagged events with  $x_L > 0.98$  (cf. section 7.1).

The elastic yield was calculated as  $N(1 - R_{diss})/\varepsilon_{el}$ , where  $N$  is the number of events passing the selection criteria presented in section 5.1 and  $R_{diss}$  is the fraction of proton-dissociative events in this sample (see section 7.1). The acceptance  $\varepsilon_{el}$  is the one determined with EPSOFT for elastic events. The proton-dissociative yield was determined from  $NR_{diss}/\varepsilon_{diss}^{el-cuts}$ , where  $\varepsilon_{diss}^{el-cuts}$  is the acceptance for proton-dissociative events when the criteria used to select the

elastic events are applied (section 5.1). Note that for  $\varepsilon_{diss}^{el-cuts}$  EPSOFT and PYTHIA agree in shape and normalisation. For the kinematic range  $50 < W < 100$  GeV,  $|t| < 0.5$  GeV<sup>2</sup> and  $(M_p + M_\pi)^2 < M_N^2 < 0.1W^2$  one obtains

$$R_{el/p-diss} = \frac{\sigma_{\gamma p \rightarrow \rho^0 p}}{\sigma_{\gamma p \rightarrow \rho^0 N}} = \frac{1 - R_{diss}}{R_{diss}} \frac{\varepsilon_{diss}^{el-cuts}}{\varepsilon_{el}} = 2.0 \pm 0.2 \text{ (stat.)} \pm 0.7 \text{ (syst.)}. \quad (21)$$

The quoted error is given by the uncertainties on  $R_{diss}$  and on the acceptance. The result was obtained assuming a mass dependence of the type  $d^2\sigma/dM_N^2 \propto 1/M_N^n$  with  $n = 2.24$  as measured by CDF [37]. Varying  $n$  by  $\pm 0.2$  induces a change of  $\pm 0.3$  in  $\sigma_{\gamma p \rightarrow \rho^0 p}/\sigma_{\gamma p \rightarrow \rho^0 N}$ ; this is not included in the quoted systematic uncertainty.

The present result is consistent with that found for  $pp$  collisions at ISR [34],  $R_{el/p-diss} = 2.08 \pm 0.13$  at a centre-of-mass energy of 53 GeV for  $M_N^2 < 0.05s_{pp}$  ( $\sqrt{s_{pp}}$  is the proton-proton centre-of-mass energy) and  $1.69 \pm 0.11$  for  $M_N^2 < 0.1s_{pp}$ . It is also consistent with the result found by the H1 Collaboration [31]:  $\sigma_{\gamma p \rightarrow \rho^0 p}/\sigma_{\gamma p \rightarrow \rho^0 N} = 1.54 \pm 0.26 \text{ (stat.)} \pm 0.31 \text{ (syst.)}$  for  $7 < Q^2 < 36$  GeV<sup>2</sup>,  $60 < W < 180$  GeV and  $M_N^2 < 0.05W^2$ . The ZEUS and H1 data together indicate that the ratio  $\sigma_{\gamma p \rightarrow \rho^0 p}/\sigma_{\gamma p \rightarrow \rho^0 N}$  is not a strong function of the photon virtuality. Our result in conjunction with the  $pp$  data and the  $ep$  results at non-zero  $Q^2$  supports the hypothesis of factorisation.

## 9 A model dependent derivation of the pion-proton cross section

As discussed earlier, the measured cross section for the process  $\gamma p \rightarrow \pi^+\pi^-p$  includes the contributions of resonant  $\rho^0 \rightarrow \pi^+\pi^-$  production, non-resonant  $\pi^+\pi^-$  production and their interference. Non-resonant  $\pi^+\pi^-$  production can be described by the photon fluctuating into a virtual  $\pi^+\pi^-$  pair with one or both pions scattering elastically off the proton. The amplitude for this process can thus be written in terms of the  $\pi p$  total cross section  $\sigma_{\pi p}$ . We have extracted this cross section in the framework of a recent calculation [41], based on Söding's approach [38], in which  $\sigma_{\pi p}$  is one of the parameters.

The total  $\pi p$  cross section was determined by fitting the calculation of ref. [41] to the  $M_{\pi\pi}$  distribution of Fig. 6. The fit gives  $\sigma_{\pi p} = 31 \pm 2 \text{ (stat.)} \pm 3 \text{ (syst.)}$  mb at an average pion-proton centre-of-mass energy  $\sqrt{s_{\pi p}} \simeq \sqrt{\langle W^2 \rangle/2} \simeq 50$  GeV. The systematic error reflects the systematic uncertainty of the data. An additional uncertainty of approximately 15% was evaluated by repeating the fit with different values of the parameters of the model. The value of  $\chi^2/ndf$  is 23.4/23.

Our result is consistent with the extrapolation of the fits by Donnachie and Landshoff [61] which give  $\sigma_{\pi p} = 26.6$  mb at  $\sqrt{s_{\pi p}} = 50$  GeV.

The predictions of the calculation [41] using the fitted value of  $\sigma_{\pi p}$  are shown in Figs. 7, 8 and 12. Both the decrease of the skewing with increasing  $|t|$  and the variation of the  $t$ -slope with  $M_{\pi\pi}$  are well described. To obtain the curves shown in Figs. 8 and 12, events were generated with a Monte Carlo program based on [41] and were binned as a function of  $M_{\pi\pi}$  and  $t$ . The fits performed to the  $M_{\pi\pi}$  spectra in the data for different  $t$  bins (using eq. (16)) and to the  $t$  distributions for different  $M_{\pi\pi}$  bins were repeated for the generated events.

## 10 Summary and conclusions

We have presented a high statistics study of  $\rho^0$  photoproduction for  $50 < W < 100$  GeV and  $|t| < 0.5$  GeV<sup>2</sup>. With respect to previous analyses at HERA, the present one features larger statistics and reduced systematic uncertainties. The main novel results can be summarised as follows:

- The  $\pi^+\pi^-$  invariant mass spectrum is skewed and the amount of skewing decreases with increasing  $|t|$ , consistent with the results from fixed target experiments.
- The cross section for resonant  $\rho^0$  production,  $\gamma p \rightarrow \rho^0 p$ , is  $11.2 \pm 0.1$  (stat.)  $^{+1.1}_{-1.2}$  (syst.)  $\mu\text{b}$  at  $\langle W \rangle = 71.7$  GeV. It increases slowly with  $W$ , exhibiting a power-like behaviour of the type  $W^a$  with  $a = 0.16 \pm 0.06$  (stat.)  $^{+0.11}_{-0.15}$  (syst.), consistent with  $a \simeq 0.22$ , the value expected for a “soft” pomeron.
- The  $t$  distribution for the reaction  $\gamma p \rightarrow \pi^+\pi^-p$  is well described by an exponential of the form  $A_{\pi\pi} \exp(-b_{\pi\pi}|t| + c_{\pi\pi}t^2)$ . The slope  $b_{\pi\pi}$  decreases rapidly with increasing  $M_{\pi\pi}$ , again consistent with the results from fixed target experiments.

The  $t$  dependence of the cross section of the reaction  $\gamma p \rightarrow \rho^0 p$  can also be described by a function of the type  $A_\rho \exp(-b_\rho|t| + c_\rho t^2)$ , with  $b_\rho = 10.9 \pm 0.3$  (stat.)  $^{+1.0}_{-0.5}$  (syst.) GeV<sup>-2</sup> and  $c_\rho = 2.7 \pm 0.9$  (stat.)  $^{+1.9}_{-1.7}$  (syst.) GeV<sup>-4</sup>.

A fit with the function  $b_\rho(W) = b_\rho(W_0) + 2\alpha_{\rho'} \ln(W/W_0)^2$  yields  $\alpha_{\rho'} = 0.23 \pm 0.15$  (stat.)  $^{+0.10}_{-0.07}$  (syst.) GeV<sup>-2</sup>, consistent with results from elastic hadron-hadron scattering.

- The  $\rho^0$  spin density matrix elements  $r_{00}^{04}$ ,  $\Re[r_{10}^{04}]$  and  $r_{1-1}^{04}$  were obtained from the angular distributions of the decay pions in the helicity frame; their values are consistent with  $s$ -channel helicity conservation. No dependence on  $M_{\pi\pi}$  or  $W$  is observed.
- Proton-dissociative  $\rho^0$  photoproduction, in which the proton diffractively dissociates into a system with mass  $M_N \lesssim 10$  GeV, exhibits dependences on  $M_{\pi\pi}$ ,  $W$ ,  $\cos\theta_h$  and  $\varphi_h$  consistent within errors with those of the elastic process. The slope of the  $t$  distribution is smaller than in the elastic reaction and for  $0.55 < M_{\pi\pi} < 1.2$  GeV and  $(M_p + M_\pi)^2 < M_N^2 < 0.1W^2$  is measured to be  $b = 5.8 \pm 0.3$  (stat.)  $\pm 0.5$  (syst.) GeV<sup>-2</sup>, using the PRT1 tagged events. In this kinematic region, the ratio of the elastic to proton-dissociative cross sections is  $2.0 \pm 0.2$  (stat.)  $\pm 0.7$  (syst.).
- A model calculation [41] based on the Söding approach [38] was fitted to the  $M_{\pi\pi}$  spectrum for the reaction  $\gamma p \rightarrow \pi^+\pi^-p$ . The fit yielded  $\sigma_{\pi p} = 31 \pm 2$  (stat.)  $\pm 3$  (syst.) mb at an average pion-proton centre-of-mass energy of approximately 50 GeV, consistent with the predictions of fits to fixed target  $\pi p$  data based on the “soft” pomeron. The model dependent uncertainty was estimated to be approximately 15%.

In  $\rho^0$  photoproduction the photon thus appears to behave like a vector meson. The  $W$  and  $t$  dependences of the cross section are those expected for elastic hadron-hadron scattering and the object mediating the interaction appears to be the same pomeron that dominates the hadron-hadron total cross section. The comparison of the elastic and the proton-dissociative reactions suggests that the coupling of the pomeron to the photon is independent of that to the proton,

as expected on the basis of factorisation. Our results indicate that the  $\rho^0$  not only carries the quantum numbers of the photon, but also its helicity in the  $s$ -channel system is equal to that of the photon. The skew of the mass shape and its  $t$  dependence can also be understood in terms of soft hadron-hadron interactions and simple quantum-mechanical interference between resonant and non-resonant production of pion pairs.

## Acknowledgements

We thank the DESY Directorate for their strong support and encouragement. We acknowledge the assistance of the DESY computing and networking staff. The remarkable achievements of the HERA machine group were essential for the successful completion of this work, and are gratefully appreciated; collaboration with the HERA group was particularly crucial to the successful installation and operation of the LPS. We would like to thank B. Hubbard, a former member of ZEUS, for his invaluable contribution to the LPS setting up and to the 1994 data taking.

It is a pleasure to also thank N.N. Nikolaev, M.G. Ryskin and Y.M. Shabelski for many stimulating discussions.

# References

- [1] For a review, see e.g. T.H. Bauer et al., Rev. Mod. Phys. **50** (1978) 261.
- [2] H. Blechschmidt et al., Nuovo Cimento **52A** (1967) 1348.
- [3] L.J. Lanzerotti et al., Phys. Rev. **166** (1968) 1365.
- [4] ABBHHM Collab., R. Erbe et al., Phys. Rev. **175** (1968) 1669.
- [5] W.G. Jones et al., Phys. Rev. Lett. **21** (1968) 586.
- [6] F. Bulos et al., Phys. Rev. Lett. **22** (1969) 490.
- [7] G. McClellan et al., Phys. Rev. Lett. **22** (1969) 374.
- [8] SBT Collab., H.H. Bingham et al., Phys. Rev. Lett. **24** (1970) 955.
- [9] SBT Collab., J. Ballam et al., Phys. Rev. Lett. **24** (1970) 960.
- [10] DESY-MIT Collab., H. Alvensleben et al., Nucl. Phys. **B18** (1970) 333.
- [11] R. Anderson et al., Phys. Rev. **D1** (1970) 27.
- [12] M. Davier et al., Phys. Rev. **D1** (1970) 790.
- [13] G. McClellan et al., Phys. Rev. **D4** (1971) 2683.
- [14] C. Berger et al., Phys. Lett. **39B** (1972) 659.
- [15] SWT Collab., Y. Eisenberg et al., Phys. Rev. **D5** (1972) 15.
- [16] J. Park et al., Nucl. Phys. **B36** (1972) 404.
- [17] SBT Collab., J. Ballam et al., Phys. Rev. **D5** (1972) 545.
- [18] SBT Collab., J. Ballam et al., Phys. Rev. **D7** (1973) 3150.
- [19] G.E. Gladding et al., Phys. Rev. **D8** (1973) 3721.
- [20] G. Alexander et al., Nucl. Phys. **B69** (1974) 445.
- [21] B. Barish et al., Phys. Rev. **D9** (1974) 566.
- [22] G. Alexander et al., Nucl. Phys. **B104** (1976) 397.
- [23] W. Struczinski et al., Nucl. Phys. **B108** (1976) 45.
- [24] R. M. Egloff et al, Phys. Rev. Lett. **43** (1979) 657.
- [25] OMEGA Photon Collab., D. Aston et al., Nucl. Phys. **B209** (1982) 56.
- [26] ZEUS Collab., M. Derrick et al., Z.Phys. **C69** (1995) 39.
- [27] H1 Collab., S. Aid et al., Nucl. Phys. **B463** (1996) 3.

- [28] ZEUS Collab., M. Derrick et al., Z. Phys. **C73** (1997) 253.
- [29] J.J. Sakurai, Phys. Rev. Lett. **22** (1969) 981.
- [30] H1 Collab., S. Aid et al., Nucl. Phys. **B472** (1996) 3;  
ZEUS Collab., J.Breitweg et al., Z. Phys. **C75** (1997) 215.
- [31] H1 Collab., C. Adloff et al., Z. Phys. **C75** (1997) 607.
- [32] For reviews, see e.g.  
G. Alberi and G. Goggi, Phys. Rep. **74** (1981) 1;  
K. Goulianos, Phys. Rep. **101** (1983) 169;  
N.P. Zotov and V.A. Tsarev, Sov. Phys. Uspekhi **31** (1988) 119;  
G. Giacomelli, Int. J. Mod. Phys. A, vol. 5, no. 2 (1990), 223.
- [33] C. Conta et al., Nucl. Phys. **B175** (1980) 97.
- [34] CHLM Collab., M.G. Albrow et al., Nucl. Phys. **B108** (1976) 1;  
CHLM Collab., J.C.M. Armitage et al., Nucl. Phys. **B194** (1982) 365;  
N. Amos et al., Phys. Lett. **B120** (1983) 460.
- [35] UA4 Collab., M. Bozzo et al., Phys. Lett. **147B** (1984) 385;  
UA4 Collab., M. Bozzo et al., Phys. Lett. **147B** (1984) 392;  
UA5 Collab., R.E. Ansorge et al., Z. Phys. **C33** (1986) 175;  
UA4 Collab., D. Bernard et al., Phys. Lett. **B186** (1987) 227.
- [36] CDF Collab., F. Abe et al., Phys. Rev. **D50** (1994) 5518.
- [37] CDF Collab., F. Abe et al., Phys. Rev. **D50** (1994) 5535.
- [38] P. Söding, Phys. Lett. **19** (1966) 702.
- [39] T. Regge, Nuovo Cimento **14** (1959) 951;  
T. Regge, Nuovo Cimento **18** (1960) 947;  
see also e.g. P.D.B. Collins, “An Introduction to Regge Theory and High Energy Physics”  
(Cambridge University Press, Cambridge 1977).
- [40] T.J. Chapin et al., Phys. Rev. **D31** (1985) 17.
- [41] M.G. Ryskin and Y.M. Shabelski, preprint hep-ph/9701407 (1997).
- [42] ZEUS Collab., M. Derrick et al., The ZEUS Detector, Status Report 1993, DESY (1993).
- [43] ZEUS Collab., M. Derrick et al., Phys. Lett. **B293** (1992) 465.
- [44] C. Alvisi et al., Nucl. Instr. Meth. **A305** (1991) 30.
- [45] N. Harnew et al., Nucl. Instr. Meth. **A279** (1989) 290;  
B. Foster et al., Nucl. Phys., Proc. Suppl. **B32** (1993) 181;  
B. Foster et al., Nucl. Instr. Meth. **A338** (1994) 254.
- [46] B. Bock et al., Nucl. Instr. Meth. **A344** (1994) 335.

- [47] M. Derrick et al., Nucl. Instr. Meth. **A309** (1991) 77;  
A. Andresen et al., Nucl. Instr. Meth. **A309** (1991) 101;  
A. Caldwell et al., Nucl. Instr. Meth. **A321** (1992) 356;  
A. Bernstein et al., Nucl. Instr. Meth. **A336** (1993) 23.
- [48] A. Bamberger et al., DESY report DESY 97-157 (1997).
- [49] ZEUS Collab., J. Breitweg et al., Z. Phys. **C75** (1997) 421.
- [50] J. Andruszków et al., DESY report DESY 92-066 (1992);  
ZEUS Collab., M. Derrick et al., Z. Phys. **C63** (1994) 391.
- [51] D. Westphal, Ph.D. thesis, Hamburg University (1997), DESY Internal Report F35D-97-11.
- [52] J. Grosse-Knetter, Ph.D. thesis, Hamburg University (1997), DESY Internal Report F35D-97-02.
- [53] ZEUS Collab., M.Derrick et al., Z. Phys. **C73** (1996) 73.
- [54] M. Kasprzak, Ph.D. thesis, Warsaw University (1996), DESY Internal Report F35D-96-16.
- [55] G. Marchesini et al., Comp. Phys. Comm. **67** (1992) 465;  
B.R. Webber, in “Proceedings of the Workshop ‘Physics at HERA’ ”, DESY, 29-30 October 1991, editors W. Buchmüller and G. Ingelman, p. 1354;  
L. Stanco, ibidem, p. 1363.
- [56] M. Arneodo, L. Lamberti and M.G. Ryskin, Comput. Phys. Commun. **100** (1997) 195.
- [57] T. Sjöstrand, Comp. Phys. Comm. **82** (1994) 74.
- [58] K. Kurek, DESY Report DESY 96-209 (1996) and private communications.
- [59] R.M. Barnett et al., Phys. Rev. **D54** (1996) 1.
- [60] M. Ross and L. Stodolsky, Phys. Rev. **149** (1966) 1172.
- [61] A. Donnachie and P.V. Landshoff, Phys. Lett. **B185** (1987) 403;  
A. Donnachie and P.V. Landshoff, Nucl. Phys. **B311** (1989) 509;  
P.V. Landshoff, Nucl. Phys. B (Proc. Suppl.) **18C** (1990) 211.
- [62] J.R. Cudell et al., preprint hep-ph 9601336 (1996).
- [63] K. Schilling et al., Nucl. Phys. **B15** (1970) 397;  
K. Schilling and G. Wolf, Nucl. Phys. **B61** (1973) 381.
- [64] M.G. Ryskin and Y.M. Shabelski, preprint hep-ph/9704279 (1997).
- [65] H. Holtmann et al., Z. Phys. **C69** (1996) 297.



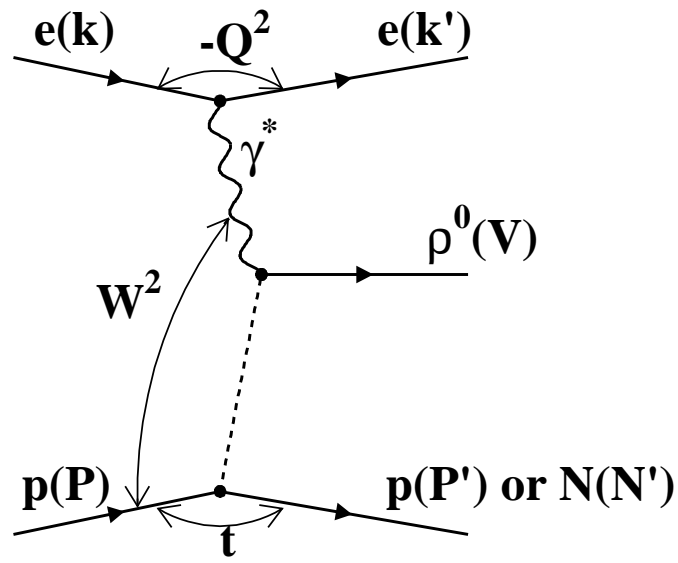


Figure 1: Elastic or proton-dissociative  $\rho^0$  production in  $ep$  collisions.

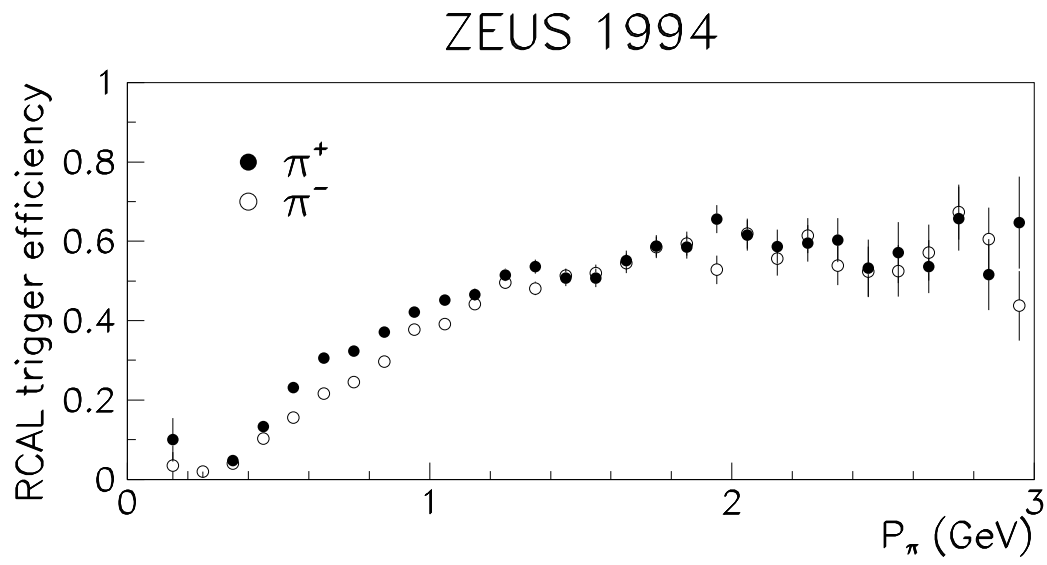


Figure 2: RCAL trigger efficiency as a function of the pion momentum  $P_\pi$ . The full symbols refer to positive pions and the open ones to negative pions. Only statistical errors are shown.

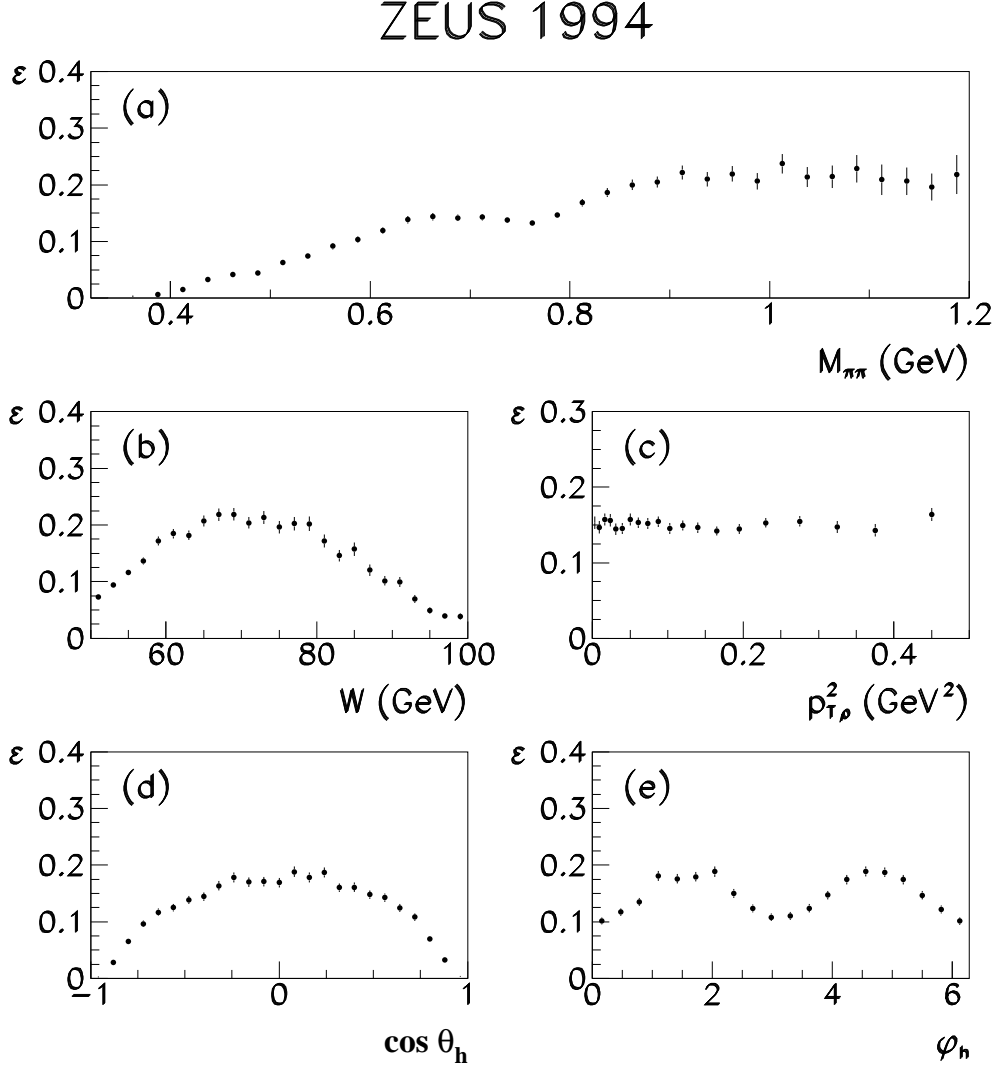


Figure 3: Overall acceptance  $\varepsilon$  for elastic  $\rho^0$  photoproduction,  $ep \rightarrow e\rho^0 p$ , as a function of (a)  $M_{\pi\pi}$ , (b)  $W$ , (c)  $p_{T\rho}^2$ , (d)  $\cos \theta_h$  and (e)  $\varphi_h$  obtained with the EPSOFT generator. Only statistical errors are shown.

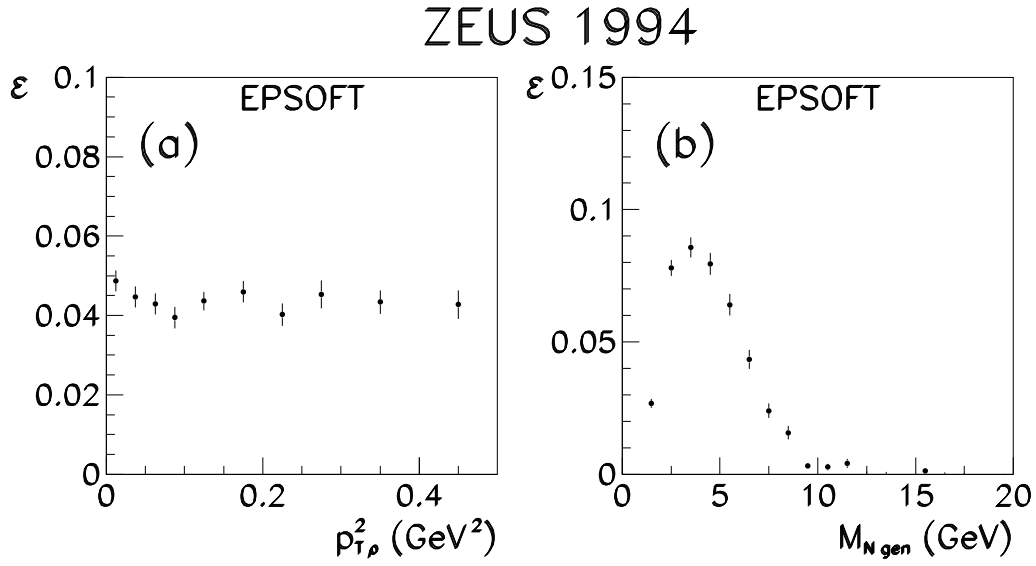


Figure 4: The overall acceptance as a function of (a)  $p_{T\rho}^2$  and (b)  $M_{Ngen}$  for proton-dissociative events,  $ep \rightarrow e\rho^0 N$ , tagged with the PRT1 (see section 5.2);  $M_{Ngen}$  indicates the generated value of  $M_N$ . Only statistical errors are shown.

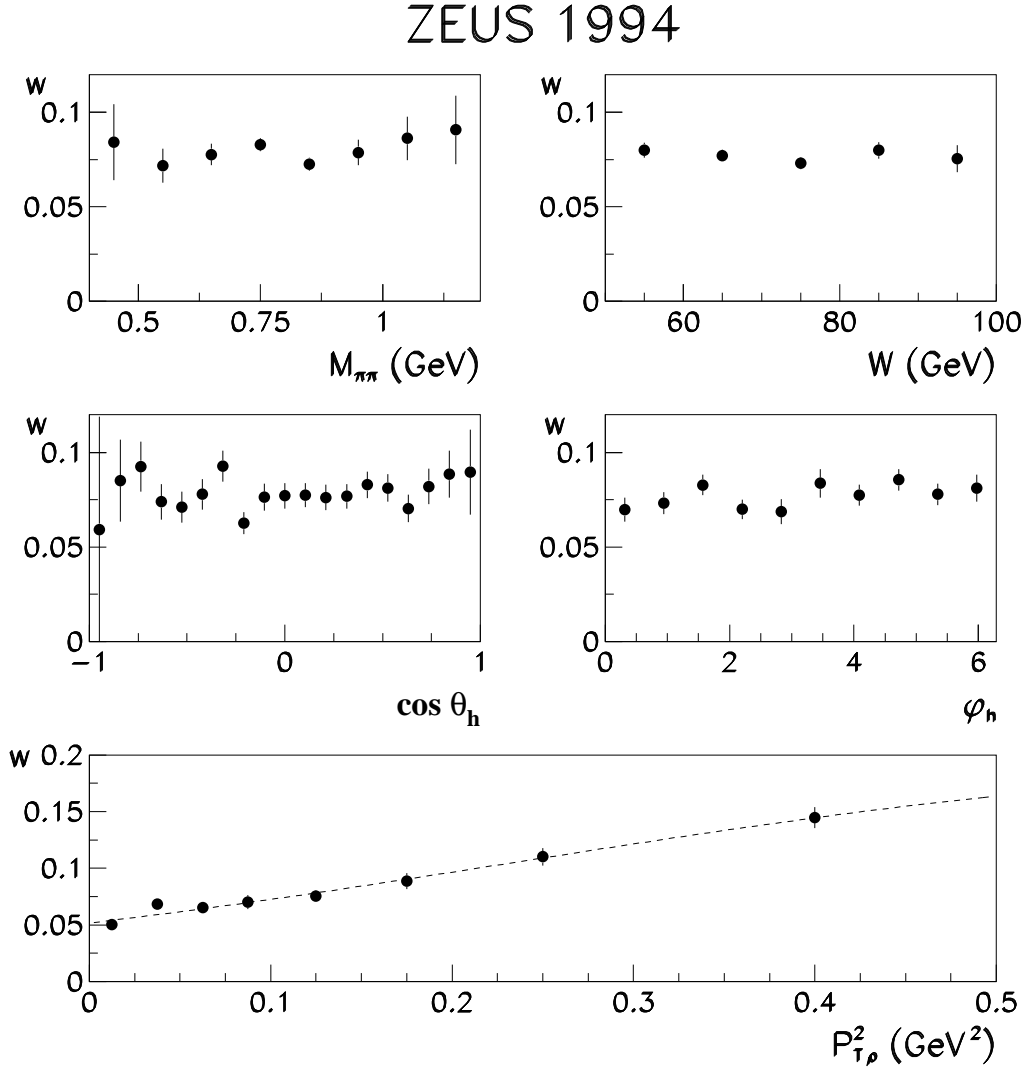


Figure 5: The ratios  $w$  of the uncorrected  $M_{\pi\pi}$ ,  $W$ ,  $\cos \theta_h$ ,  $\varphi_h$  and  $p_{T\rho}^2$  distributions for the proton-dissociative sample (PRT tagged) and the sample obtained with the elastic cuts. Only statistical errors are shown. The dashed line is the result of the fit with equation (7).

# ZEUS 1994

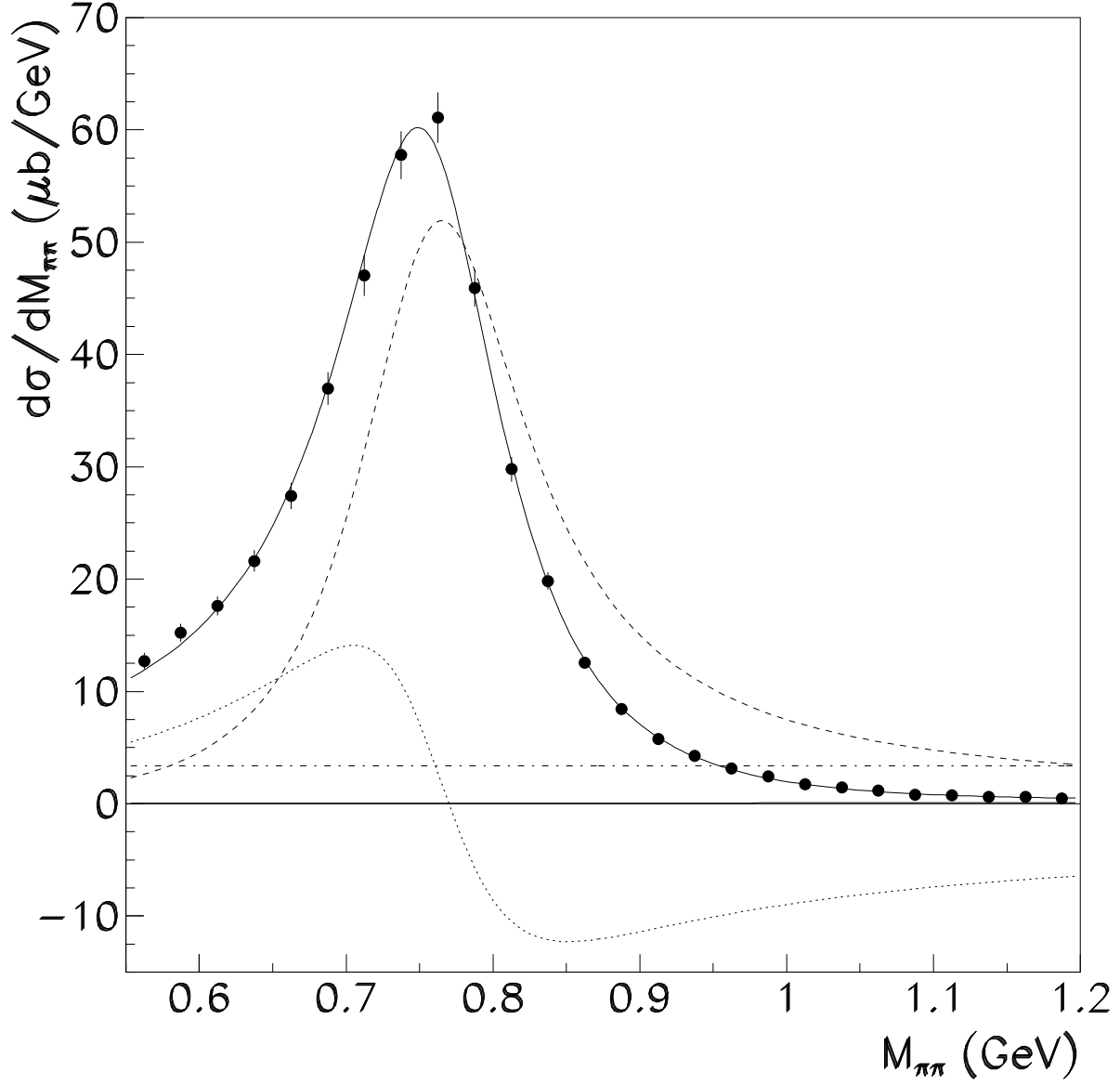


Figure 6: The differential cross section  $d\sigma/dM_{\pi\pi}$  for the elastic reaction  $\gamma p \rightarrow \pi^+\pi^-p$  in the kinematic region  $50 < W < 100 \text{ GeV}$  and  $|t| < 0.5 \text{ GeV}^2$ . The points represent the ZEUS data and the curves indicate the result of the fit to the data using expression (15). The dashed curve represents the resonant contribution, the dot-dashed curve the non-resonant contribution and the dotted curve the contribution of the interference term. The continuous curve is the sum. Only statistical errors are shown.

# ZEUS 1994

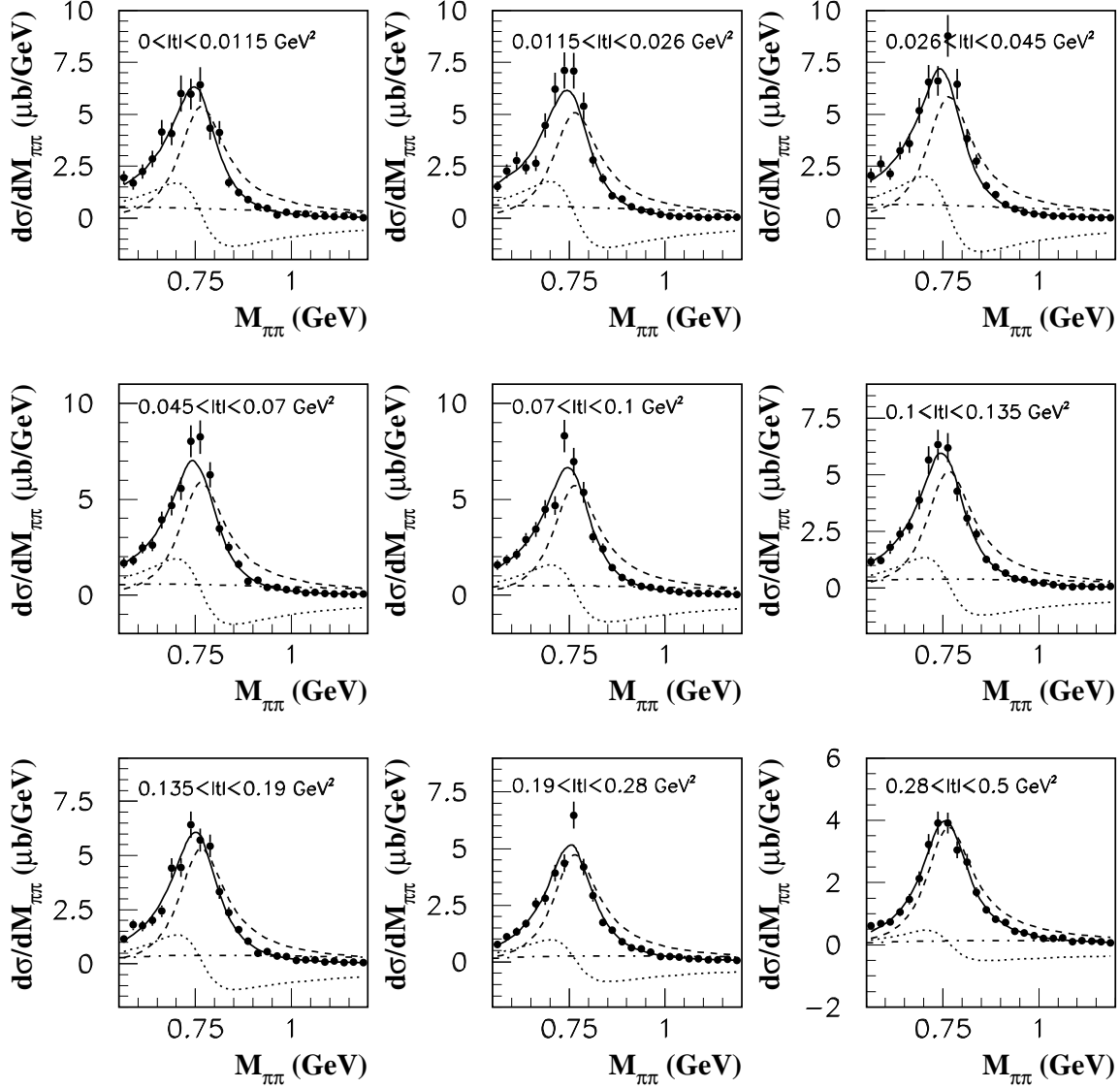


Figure 7: The differential cross sections  $d\sigma/dM_{\pi\pi}$  for the elastic reaction  $\gamma p \rightarrow \pi^+\pi^-p$  in the range  $50 < W < 100$  GeV for different  $|t|$  bins. The points represent the ZEUS data and the curves indicate the results of the fit to the data based on the model of ref. [41] (cf. section 9). The dashed curve represents the resonant contribution, the dot-dashed curve the non-resonant contribution and the dotted curve the contribution of the interference term. The continuous curve is the sum. Only statistical errors are shown.

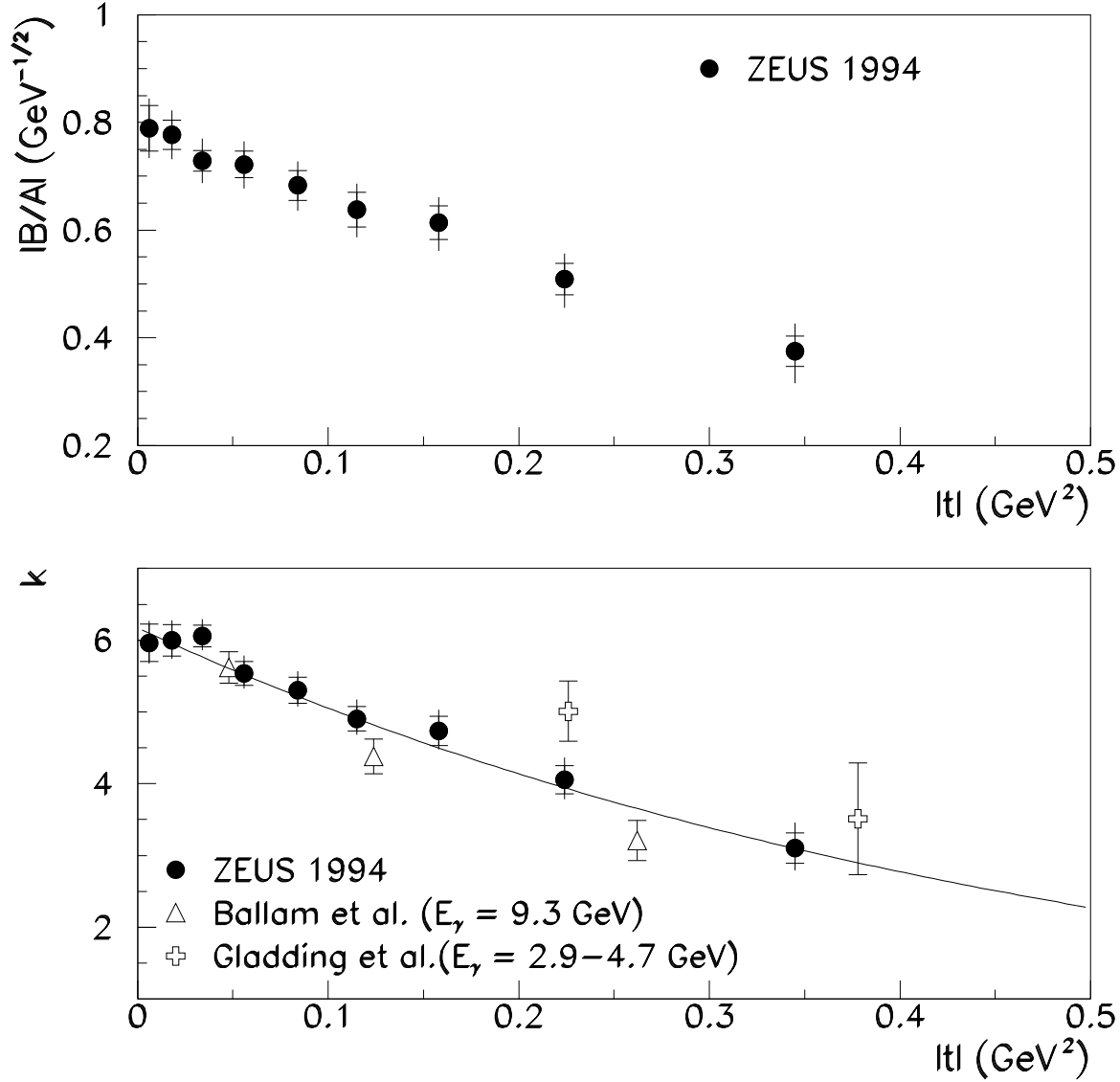


Figure 8: The ratio  $|B/A|$  (upper plot) and the parameter  $k$  (lower plot) as a function of  $|t|$  obtained by fitting eq. (15) and eq. (16), respectively, to the points of Fig. 7 for the elastic reaction  $\gamma p \rightarrow \pi^+ \pi^- p$  in the region  $50 < W < 100$  GeV. The solid points represent the ZEUS measurements. The inner error bars indicate the statistical uncertainty, the outer ones the statistical and systematic uncertainties added in quadrature. The results of the fixed target experiments [18] and [19] (labelled “Ballam et al.” and “Gladding et al.”, respectively) are also shown. The continuous line indicates the effective expectation of the Söding model as implemented in the calculation by Ryskin and Shabelski [41] (cf. section 9).



# ZEUS 1994

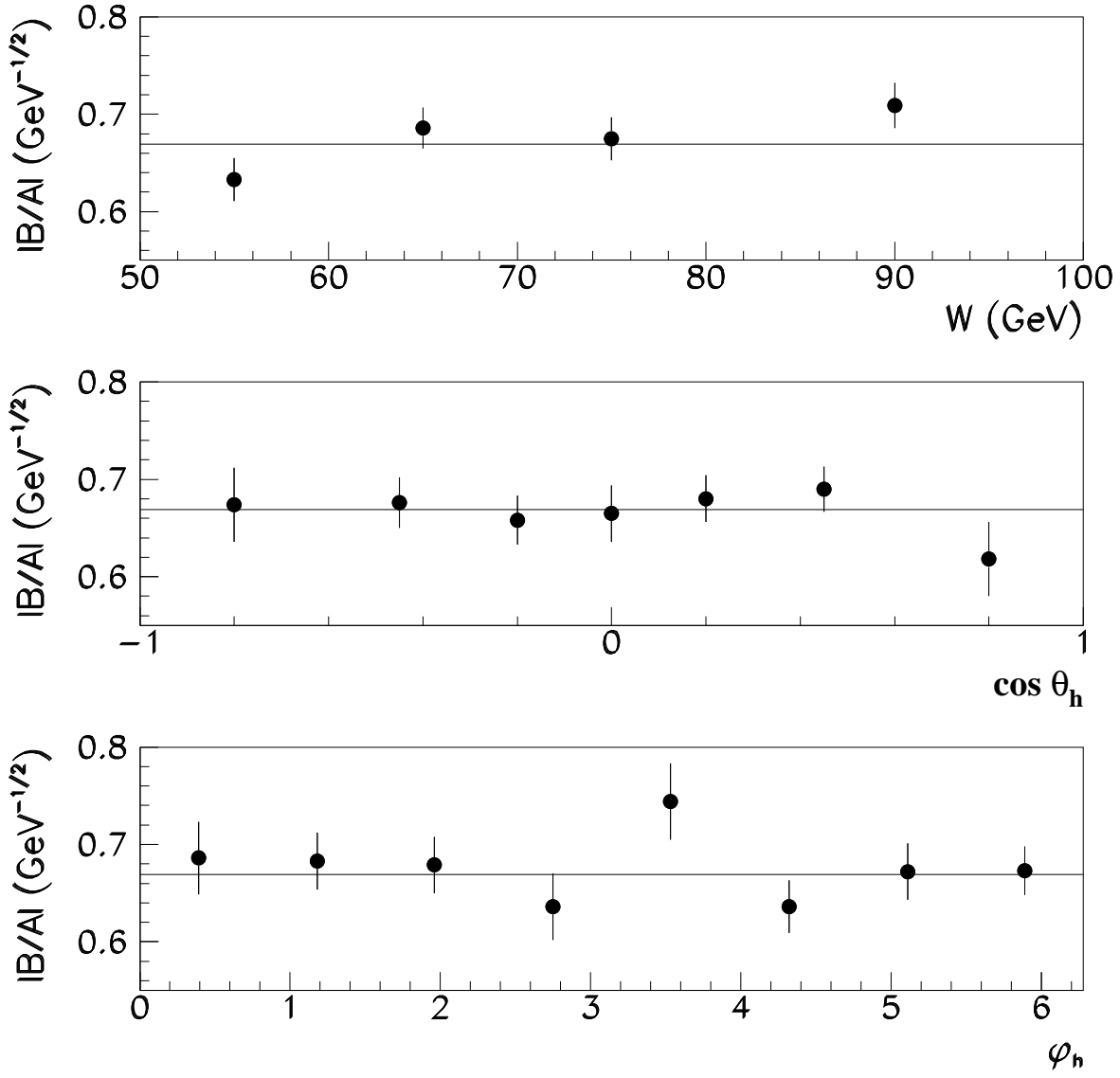


Figure 9: The ratio  $|B/A|$  as a function of  $W$ ,  $\cos \theta_h$  and  $\varphi_h$  for the elastic reaction  $\gamma p \rightarrow \pi^+ \pi^- p$  in the kinematic range  $0.55 < M_{\pi\pi} < 1.2 \text{ GeV}$ ,  $50 < W < 100 \text{ GeV}$  and  $|t| < 0.5 \text{ GeV}^2$ . Statistical errors only are shown. The continuous lines indicate the average value of  $|B/A|$ .

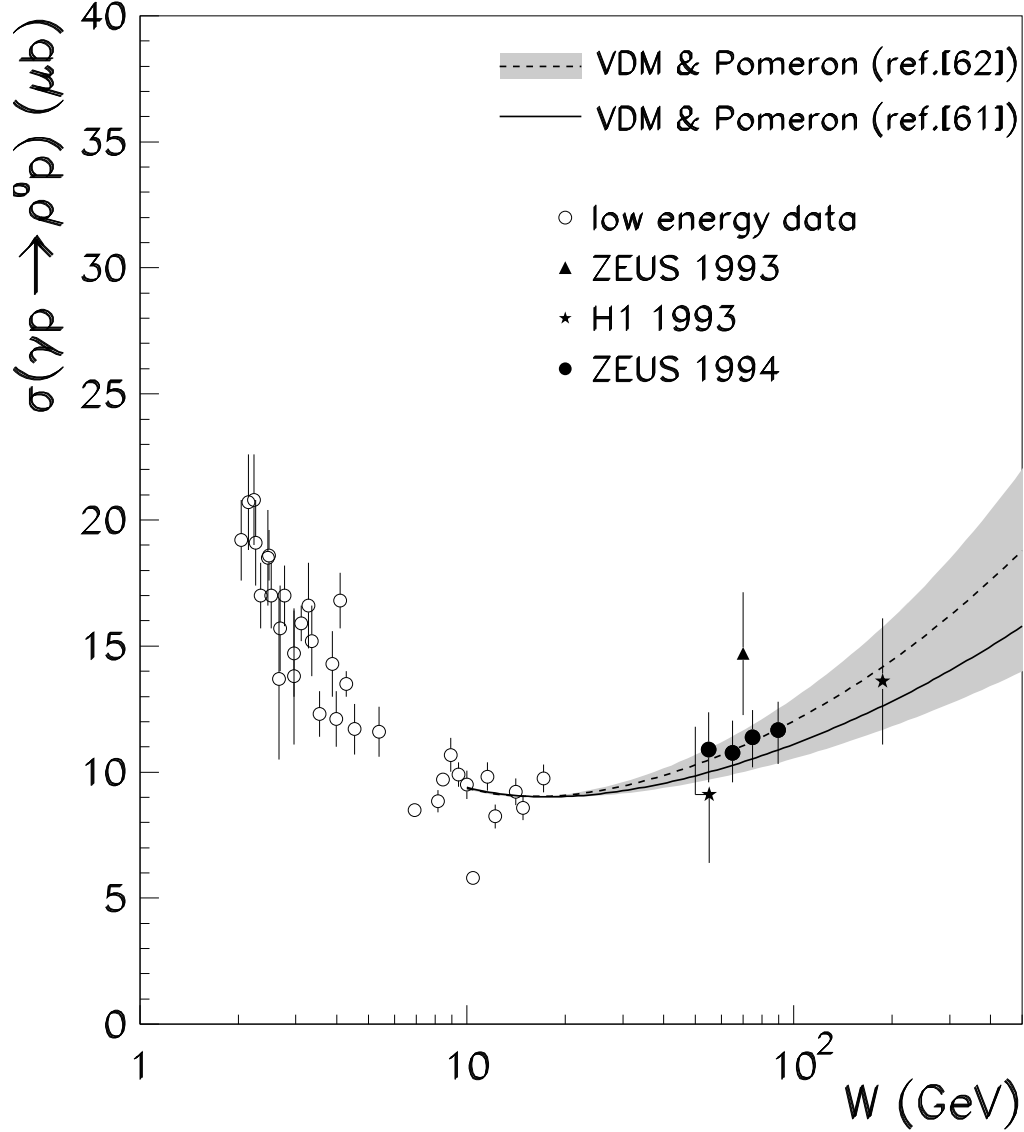


Figure 10: The integrated cross section  $\sigma_{\gamma p \rightarrow \rho^0 p}$  as a function of the centre-of-mass energy  $W$ . The ZEUS results are given for the range  $2M_\pi < M_{\pi\pi} < M_\rho + 5\Gamma_0$ ,  $|t| < 0.5 \text{ GeV}^2$ . The other results from HERA [26, 27] and a compilation of low energy data [14]-[19], [23]-[25] are also shown. The continuous and dashed line are parametrisations [52] based on Regge theory which assume the value of the pomeron intercept found by Donnachie and Landshoff [61] and by Cudell et al. [62], respectively. The band corresponds to the uncertainty in the determination of the pomeron intercept of ref. [62]. The error bars of the ZEUS points indicate the sum of statistical and systematic uncertainties in quadrature. For the points at the same value of  $W$ , the error bars have been offset.

# ZEUS 1994

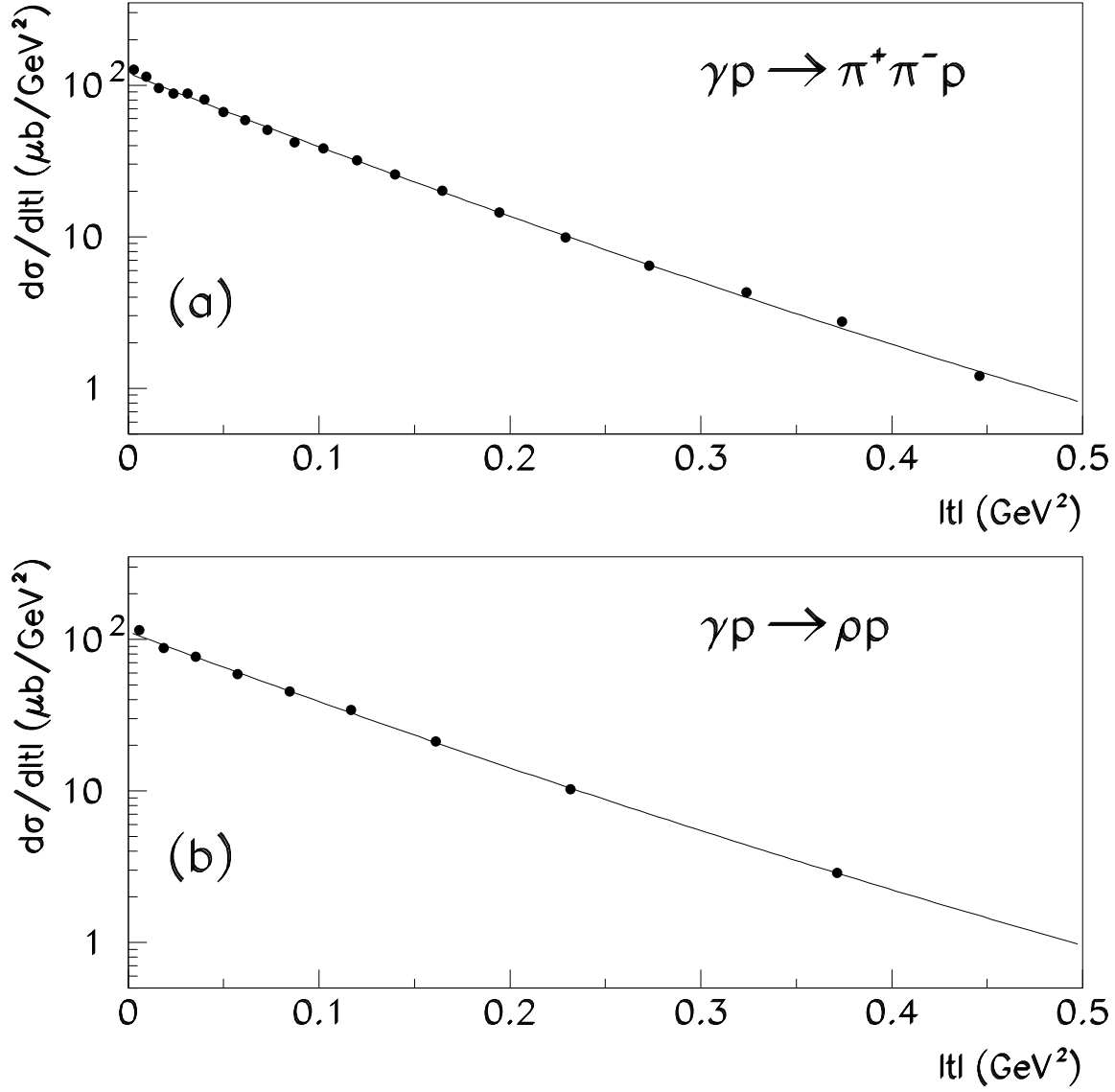


Figure 11: (a) The differential cross section  $d\sigma/d|t|$  for the process  $\gamma p \rightarrow \pi^+ \pi^- p$  in the kinematic range  $0.55 < M_{\pi\pi} < 1.2$  GeV and  $50 < W < 100$  GeV. (b) The differential cross section  $d\sigma/d|t|$  for the process  $\gamma p \rightarrow \rho^0 p$  in the kinematic range  $2M_\pi < M_{\pi\pi} < M_\rho + 5\Gamma_0$  and  $50 < W < 100$  GeV. The continuous lines in (a) and (b) represent the results of the fits with the functional forms (17) and (18), respectively. The error bars represent only the statistical uncertainties and are smaller than the size of the symbols.

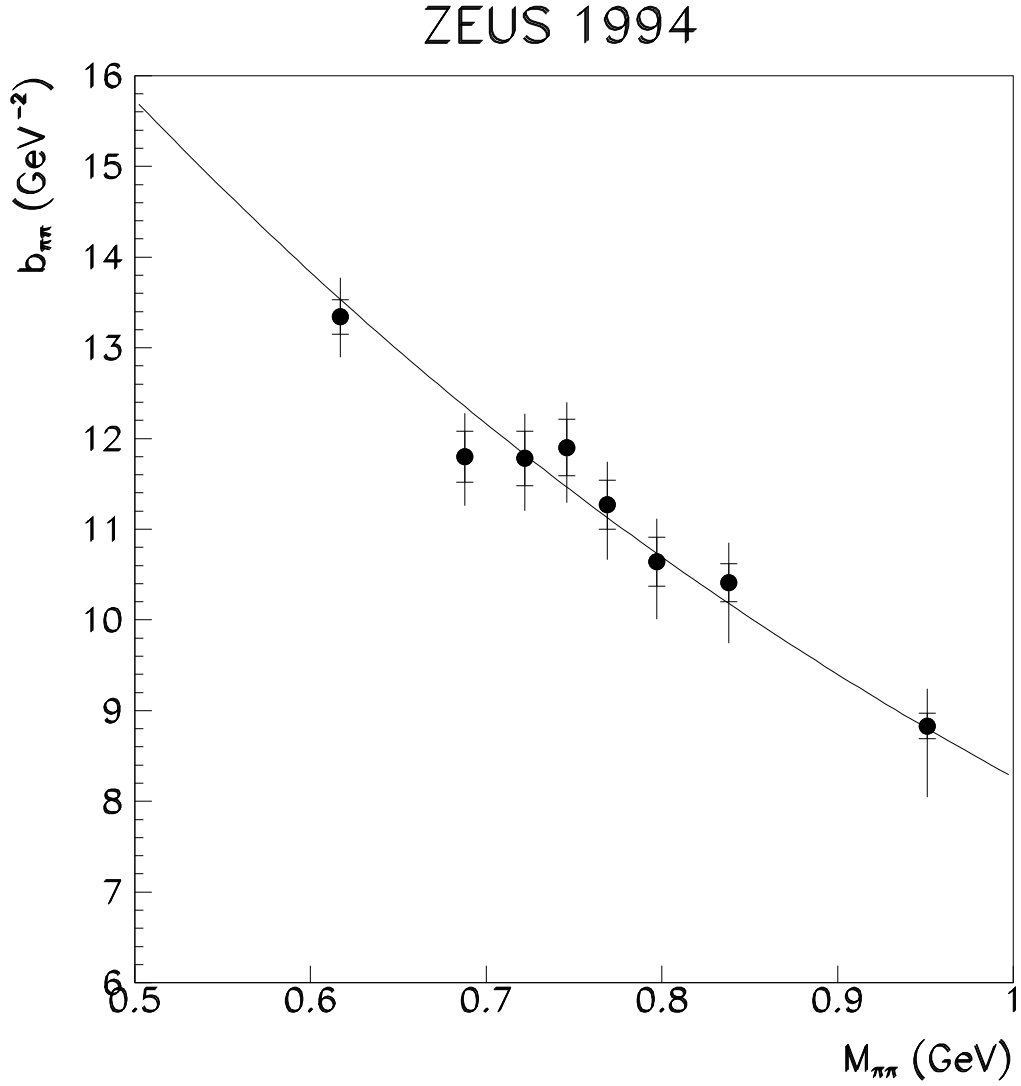


Figure 12: The slope  $b_{\pi\pi}$  resulting from a fit of equation (17) to the  $t$  distribution for the reaction  $\gamma p \rightarrow \pi^+ \pi^- p$  in different mass bins. The kinematic range is  $50 < W < 100$  GeV and  $|t| < 0.5$  GeV<sup>2</sup>. The continuous line indicates the effective expectation of the Söding model as implemented in the calculation by Ryskin and Shabelski [41] (cf. section 9). The inner bars indicate the statistical uncertainty and the outer ones the statistical and systematic uncertainties summed in quadrature.

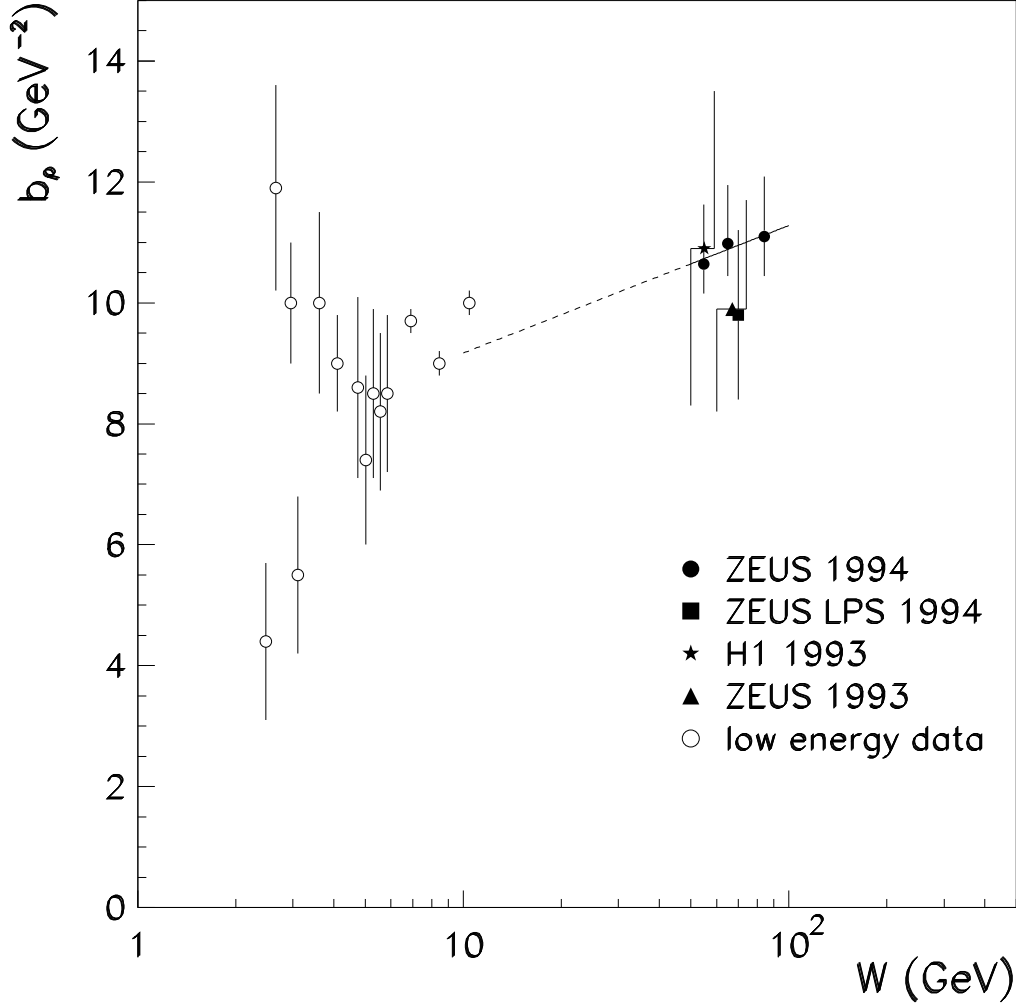


Figure 13: The slope  $b_\rho$  for the elastic reaction  $\gamma p \rightarrow \rho^0 p$  in the kinematic region  $50 < W < 100$  GeV and  $|t| < 0.5$  GeV<sup>2</sup> as a function of  $W$  together with the other recent results from HERA [26, 27, 28] and a compilation of low energy data [25, 5, 14, 19, 17]. The continuous line shows the result of the fit discussed in the text; the extrapolation of the fit to the low  $W$  region is indicated by the dashed line. The error bars of the HERA data indicate the statistical and systematic uncertainties summed in quadrature. For the points at the same value of  $W$ , the error bars have been offset.

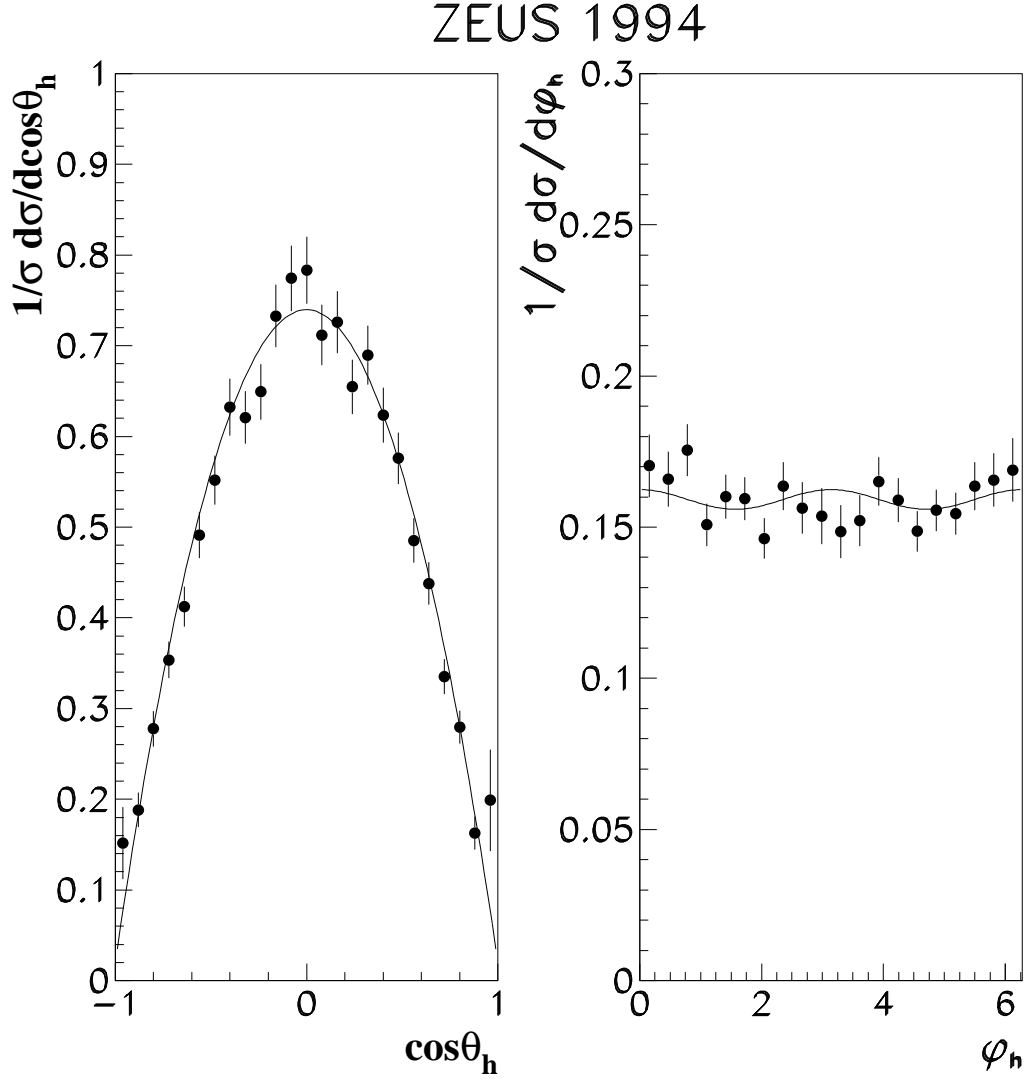


Figure 14: The differential distributions  $(1/\sigma)(d\sigma/d\cos\theta_h)$  and  $(1/\sigma)(d\sigma/d\varphi_h)$  for the reaction  $\gamma p \rightarrow \pi^+\pi^-p$  in the kinematic region  $50 < W < 100$  GeV and  $|t| < 0.5$  GeV<sup>2</sup>. The continuous lines represent the results of the fit discussed in the text. Only statistical errors are shown.

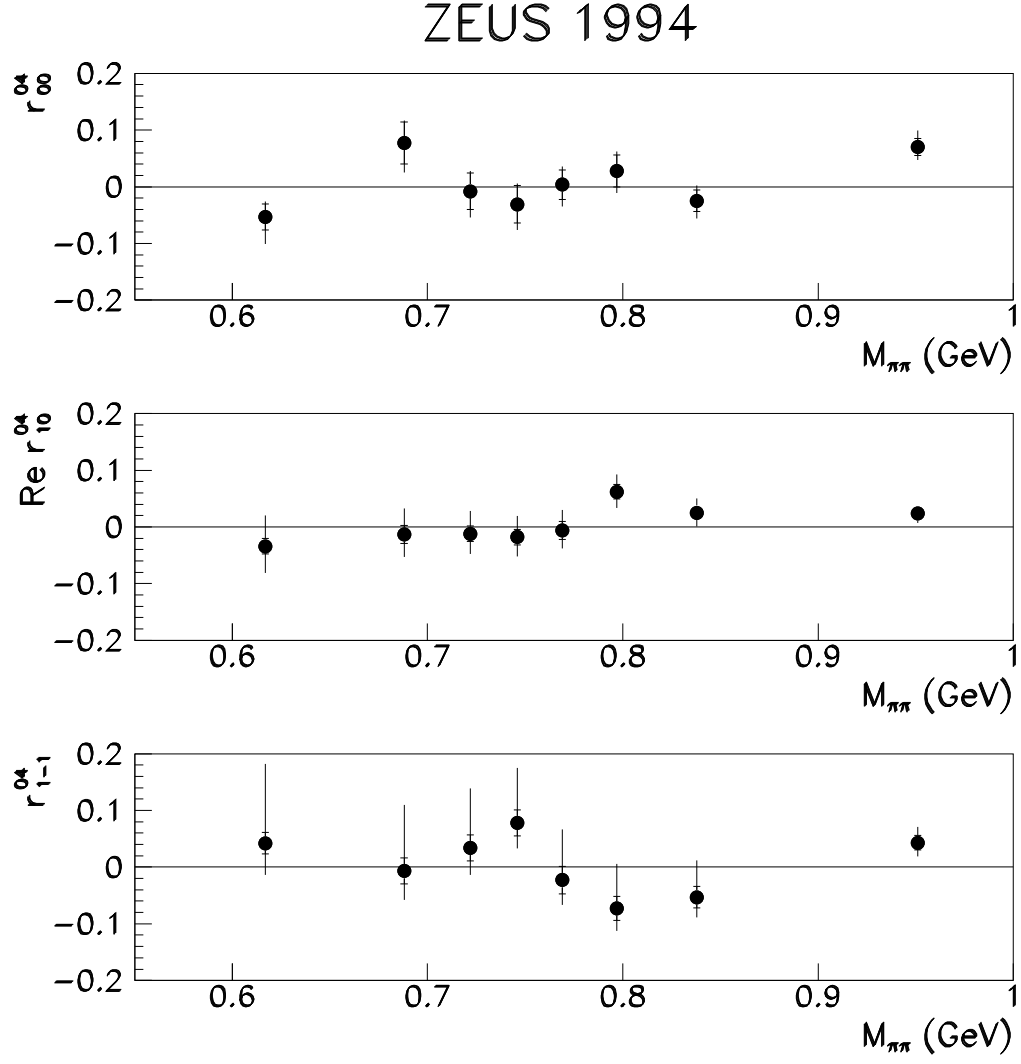


Figure 15: The results for  $r_{00}^{04}$ ,  $\Re[r_{10}^{04}]$  and  $r_{1-1}^{04}$  as a function of  $M_{\pi\pi}$  for the reaction  $\gamma p \rightarrow \pi^+ \pi^- p$  in the kinematic range  $0.55 < M_{\pi\pi} < 1.2$  GeV,  $50 < W < 100$  GeV and  $|t| < 0.5$  GeV<sup>2</sup>. The inner bars indicate the statistical uncertainty and the outer ones the statistical and systematic uncertainties summed in quadrature.

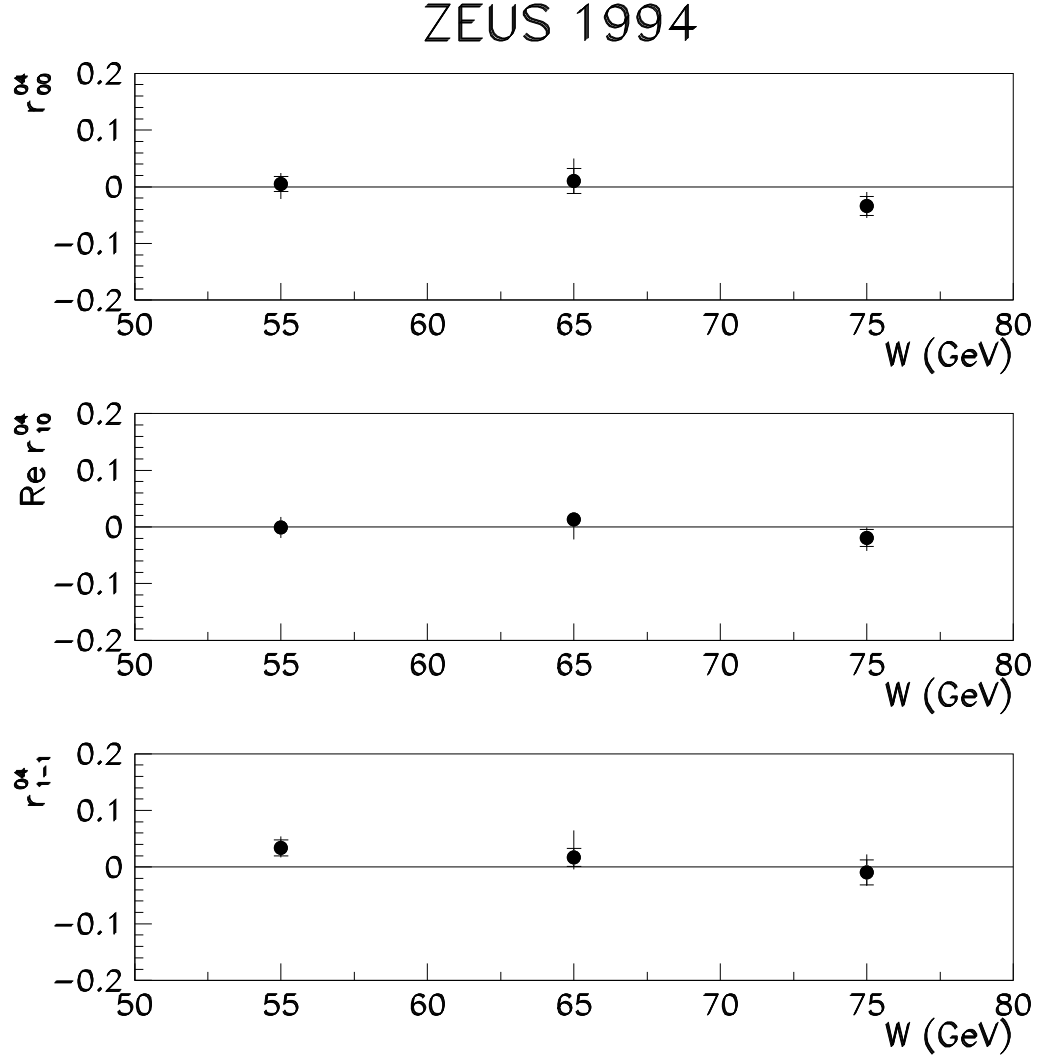


Figure 16: The results for  $r_{00}^{04}$ ,  $\Re[r_{10}^{04}]$  and  $r_{1-1}^{04}$  as a function of  $W$  for the reaction  $\gamma p \rightarrow \pi^+ \pi^- p$  in the kinematic range  $0.55 < M_{\pi\pi} < 1.2$  GeV,  $50 < W < 80$  GeV and  $|t| < 0.5$  GeV<sup>2</sup>. The inner bars indicate the statistical uncertainty and the outer ones the statistical and systematic uncertainties summed in quadrature.



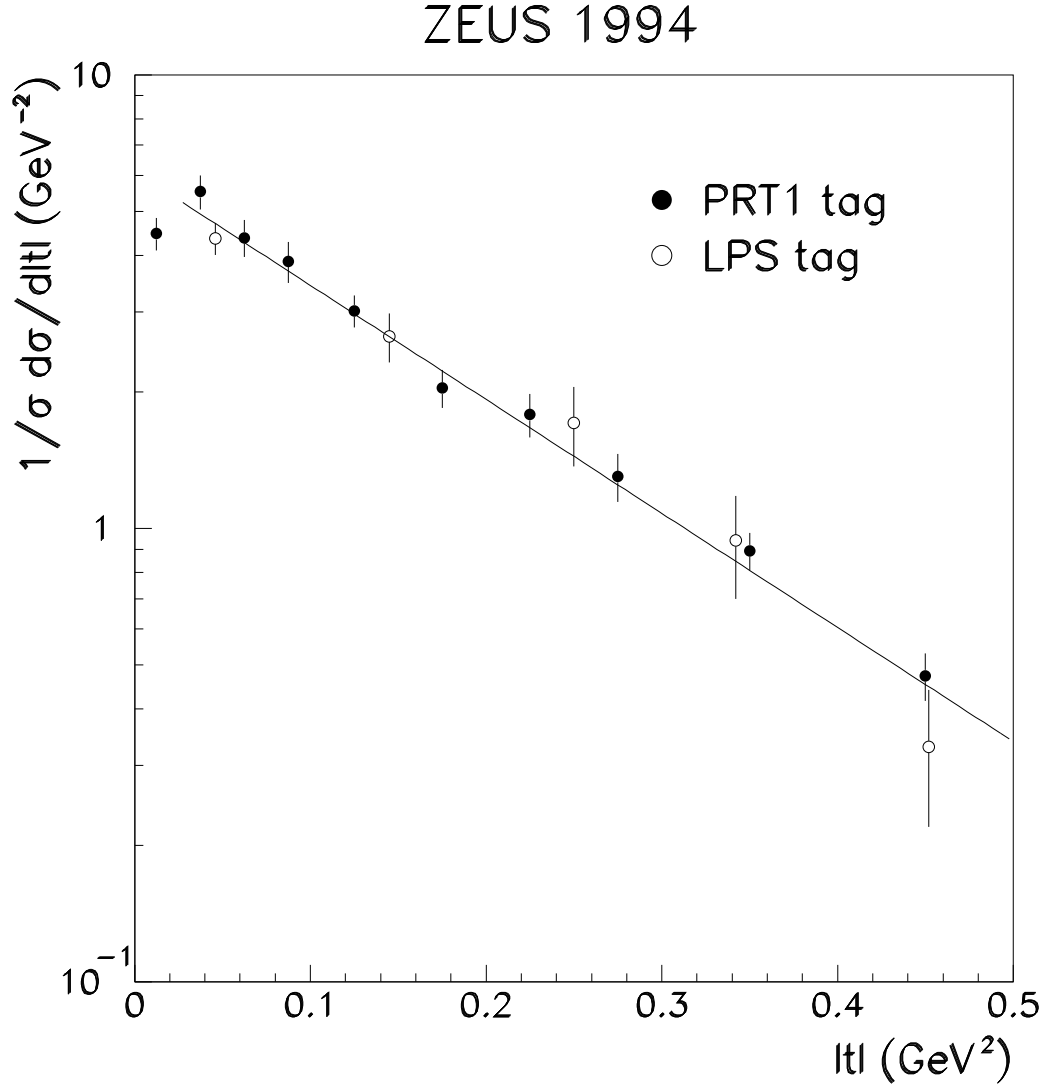


Figure 17:  $t$  distribution for the reaction  $\gamma p \rightarrow \pi^+ \pi^- N$  tagged with the PRT1 (full symbols) and with the LPS ( $x_L < 0.98$ , open symbols) in the region  $0.55 < M_{\pi\pi} < 1.2$  GeV,  $50 < W < 100$  GeV,  $|t| < 0.5$  GeV<sup>2</sup> and  $(M_p + M_\pi)^2 < M_N^2 < 0.1W^2$ . The dip at low  $|t|$  is a consequence of  $t_{\min}$  being non-zero at large values of  $M_N$ . Only statistical errors are shown. The line shows the result of the fit to the PRT1 points described in the text.